JOURNAL OF COMPUTATIONAL BIOLOGY
Volume 26, Number 3, 2019

Pp. 241–265
DOI: 10.1089/cmb.2018.0205

Cell Modeling Based on Bubbles with Weighted Membranes

YUANDI WANG,[1] QINGMEI WEN,[1] ZHIGANG ZHOU,[2] and NANJUN YAN[1]

ABSTRACT

Mathematicization for cell modeling provides an effective tool to verify the biological theory, and the existing research mainly focuses on the description of cell structures. This article then addresses the pattern question of cell division or morphogenesis by means of bubble model with weighted membranes. In this study, we show that cell shapes including intersection angles at junction points depend on weights on membranes. For convenience, adhesion and contractile force are considered together as a factor in construction of patterning model. This model is also used to compare with experimental data. And the consistency between our model and experiments is also obtained consequently. This system of differential equations with their boundary conditions theorizes the existing experimental models, and improves the rationality of these models.

Keywords: bubble, cell pattern, differential equation model, variational principle.

1. INTRODUCTION

This article shows a cell structural model of three kinds of green algae. The research on green algae is of great significance, because some researchers agree that charophycean green algae are the closest extant protist relatives of the land plants (embryophytes). Karol et al. (2001) pointed out that the embryophytes (land plants) have long been thought to be related to the green algal group Charophyta, though the nature of this relationship and the origin of the land plants have remained unresolved.

The cell model of green algae varies with each type, for instance, *Coleochaete* and *Pediastrum* exemplify two ways of cell division (Millington et al., 1981; Ruhfel et al., 2014; Haig, 2015). Enlargement of *Coleochaete* thallus is entirely caused by the division of peripheral cells when the size of cells increases to two times for the size of the original cells while the dividing wall is perpendicular to the cell boundary (Wesley, 1928).

Cells of *Coleochaete* grow during the division process (Dupuy et al., 2010; Besson and Dumais, 2011), whereas cells of *Pediastrum* grow beginning with zoospores until they all reach full size (Gawlik and Millington 1969; Millington et al., 1981). Each *Pediastrum* cell can generate a daughter autocolony with exactly the same number and arrangement of cells as the parent colony. *Tetrastrum*, another genus of green algae, is similar to *Pediastrum* (Ahlstrom and Tiffany, 1934; Krienitz and Wachamuth, 1991).

[1]Department of Mathematics, Shanghai University, Shanghai, China.
[2]College of Aqua-life Sciences and Technology, Shanghai Ocean University, Shanghai, China.

The mechanism of cell division is an important research topic in biology, but it is difficult to describe the division in each step because of its complexity. This article proposes a model describing the growth of cells of *Pediastrum* by keeping the sum of all length of edges (including inner walls) shortest. Mathematically, it can be understood by keeping new walls shortest in *Coleochaete* cell division and by keeping the sum of all edge lengths shortest in *Pediastrum* cell division, respectively.

The geometrical shape of *Coleochaete* optimizes the building of cell walls. Biologists believe that the division orientation of most plant cells can be predicted by their shapes. Hofmeister in 1863 noted that a new cell wall is usually perpendicular to the axis of maximal cell division. Léo Errera further said that most of new cell walls of the plant cell division usually follow the shortest path (Smith, 2001), often referred to as Errera's rule. This opinion has also been verified by some experiments (Rasmussen et al., 2013; Fukushima et al., 2015). There are some important findings, for example, Sinnott and Bloch (1940) pointed out that cells split according to the phenomenon of radial division.

Recent researches have also deepened the relationship between geometry and the model based on Errera's rule. Dupuy et al. (2010) and Besson and Dumais (2011) showed that the selection of plane of division involves a competition between alternative configurations whose geometries represent local area minima.

In contrast, Wang et al. (2015) tried to explain the cell division of *Coleochaete* based on the geometrical problem of regional segmentation, which provides a mathematical model in the form of parametric equation to describe dividing flat domains with more complex boundaries, especially for some nonconvex domains. The ''regional segmentation'' was initially raised by Wiener (1914) and he proved that ''the shortest line passing through two given points on the boundary of a given circle, dividing the area of the circle in a given ratio, is an arc of a circle.'' Goldberg (1969) then generalized the problem that ''Given a convex quadrilateral, find the shortest curve which divides it into two equal areas.'' This problem is still unsolved (Klamkin, 1992). The system of equations and their boundary value conditions in the study of Wang et al. (2015) were consistent with the Cartesian coordinate form by Besson and Dumais (2011). And, this method in parametric form was also applied to simulate the expanding process for the nonuniform division, and they discuss the formational mechanism of the outer boundary (Wang and Cong, 2016; Wang and Zeng, 2018). Owing to the shortest wall mode, *Coleochaete* can adjust its strategy of cell division according to the environmental changes at any time, which is conducive for its evolution (Yang, 1986; Timme and Delwiche, 2010).

The division model like *Pediastrum* cells needs to be further theorized. Unlike *Coleochaete*, *Pediastrum* seems to have a more optimal division option. In the division process, *Coleochaete* only pursues the shortest wall, whereas the latter considers the minimal length for the entire cell borders, including outer boundaries and walls between cells. *Pediastrum* follows an early prefabricated growth mode in which the arrangement of all cells is fixed.

The bubble model can be adopted to explain the cell division of *Pediastrum*. The planar (two-dimensional) double bubble conjecture, which held that the familiar double soap bubble provides the least-length way to enclose and separate two given volumes of air, was proved by an undergraduate research geometry group supervised by Morgan (Foisy et al., 1993). Morgan's another group of undergraduates (Cox et al., 1994) proved that the perimeter of the standard triple bubble is the shortest among enclosures of connected regions. Wichiramala (2004) gave a weak approach to prove the planar triple bubble conjecture.

The bubble model was also used to discuss the shaping mechanism of *Drosophila* cells. Hayashi and Carthew (2004) introduced the bubble model to investigate the compound eye of *Drosophila*. But Käfer et al. (2007) believed that cells differ greatly from bubbles in both their membrane and internal composition since surface tension was shown to be determined to a large extent by the cortical cytoskeleton. Adhesive cells have a tendency to increase their contact interfaces, not to minimize them.

The analysis on the experimental data (released by Ahlstrom and Tiffany, 1934; Maître et al., 2012; Chan et al., 2017) proves that the real process of cell division is far more complex than the mathematical model.

One typical problem is that the outer angles on the cell boundary of *Pediastrum*, *Tetrastrum*, and of the *Drosophila* eye are not exactly the same as described in the bubble models. It is considered for *Drosophila* to be the result from the different roles of two Cadherins: E-Cadherin and N-Cadherin, and the analysis can be found in Section 6. The distribution (Fig. 1) shows a diversity for the central tendency, in which

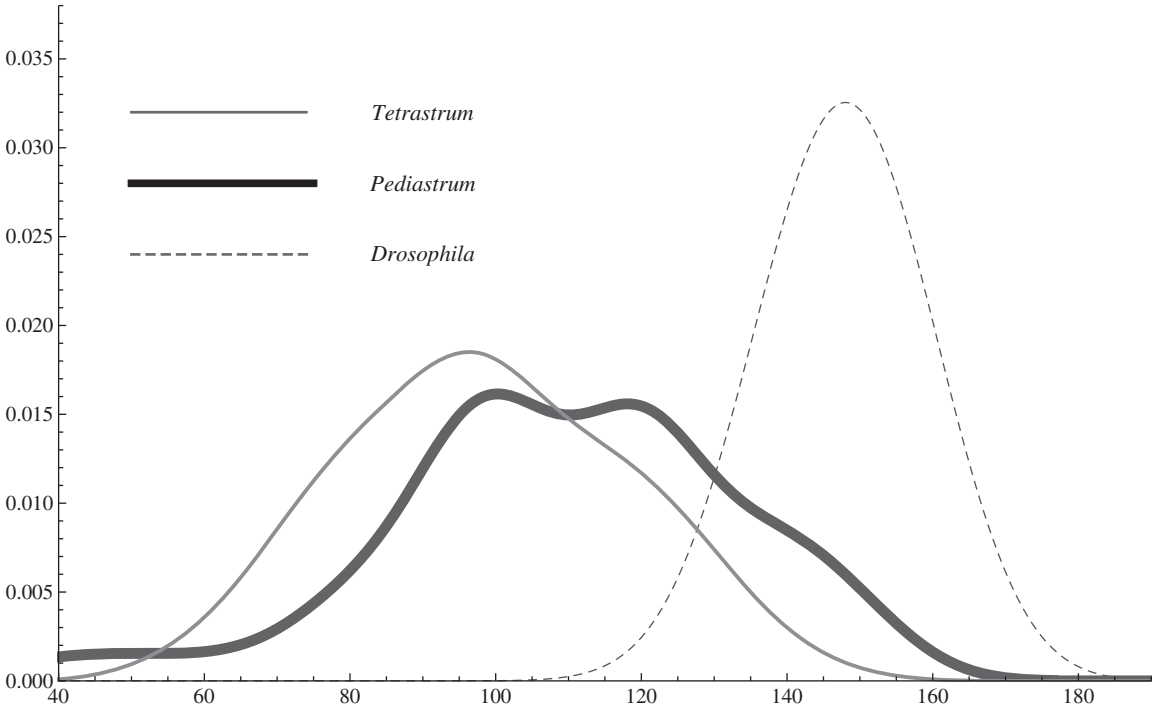

FIG. 1. Results express the comparison of three distributions, in which the horizontal axis represents the magnitude of the external angle (°).

Drosophila has a compact shape and *Tetrastrum* has a wide spread. The mean value, standard deviation, and the kurtosis of each distribution are, respectively, as listed in Table 1, which shows that the outer angles of the two algae expand widely (comparing with the retina cells of *Drosophila*). One reason is that the shape of the outer cells is influenced by flagella on boundaries, especially for *Pediastrum* cells.

To develop the theoretic analysis on cell formation, this article uses variational method to clarify the effect of surface tension and viscosity on cell shape, in particular, on its outer angle. The equations that the cell edges (the boundaries and the walls) should satisfy and corresponding boundary value conditions are deduced in this article, which provides an exact characterization of the pattern of the colony of cells, especially a mathematical description for the included angle at the intersection for edges.

This article is organized as follows: Section 2 states the system of equations and their boundary conditions. Section 3 presents the numerical simulations based on the model used in this article, and more discussions are given in Section 4. The detailed deduction process and some experimental data can be found in Sections 5 and 6 and Supplementary Materials.

2. BUBBLE MODEL WITH WEIGHTED MEMBRANES

A rule named ''sharing principle'' means two neighbor cells (with the same area) share a part of common wall as long as possible such that the total length of their boundaries and wall is minimum. There are two

Table 1. The Mean Values and Standard Deviations and the Kurtosis for Three Distributions

Item	*Mean*	*Standard deviation*	*Kurtosis*	*Skewness*
Drosophila	147.73	9.054	–0.274	–0.096
Pediastrum	109.13	24.060	0.587	–0.554
Tetrastrum	98.67	19.115	–0.589	0.0865

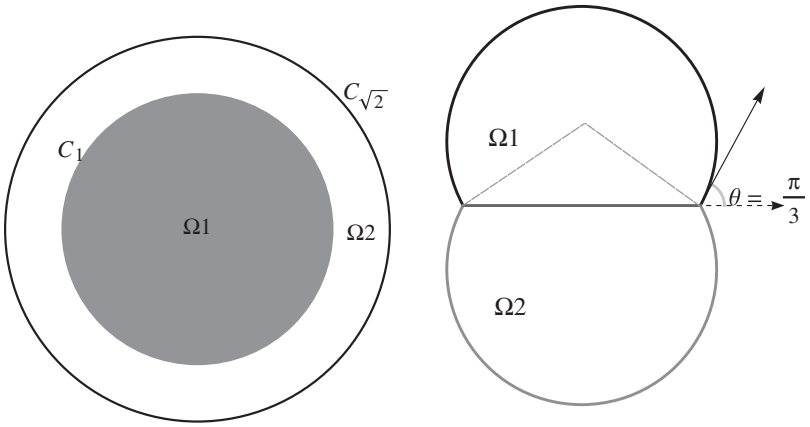

FIG. 2. Two kinds of cell models with sharing membrane: concentric circle model (left) and bubble model (right).

models satisfying ''sharing principle'': one is concentric circle model and the other one is bubble model (Fig. 2). Obviously, the total length l_c for concentric circle model is longer than that of bubble model. A simple computation shows the ratio of their lengths is

$$\frac{l_c}{l_b} = \frac{3\left(1+\sqrt{2}\right)\sqrt{\pi\left(3\sqrt{3}+8\pi\right)}}{9+8\sqrt{3}\pi} \doteq 1.34581.$$

Therefore, the bubble model is the only cell model discussed in the following discussion. For convenience, the outer surfaces (membranes) are called ''boundaries'' and the inner surfaces (membranes) are called ''walls.''

Käfer et al. (2007) pointed out that cell adhesion and cortex contractility determine cell patterning in the *Drosophila* retina. The task of this research is to find how these two factors affect the pattering. In the construction of the cell model, the difference between adhesion and tension of cell walls and the outer edges (boundaries) of the cell are considered as dominant for cell pattering because walls and edges have different environment around them.

For simplicity, our focus is on a colony containing two cells.

For a colony consisting of two cells Ω_1 and Ω_1 with it boundary $L_a \cup L_c$ (refer Fig. 3), we assume that the two (outer) boundaries L_a and L_c (the boundary of the colony) can be denoted as

$$L_a : \begin{cases} x = \varphi(t), \\ y = \psi(t), \end{cases} \quad t \in [0,\ t_*]; \qquad L_c : \begin{cases} x = p(t), \\ y = q(t), \end{cases} \quad t \in [t_c,\ T]; \tag{1}$$

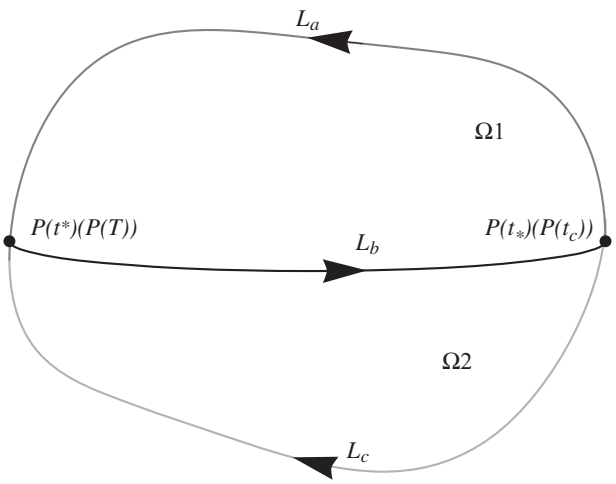

FIG. 3. Two cell model with fixed total length.

and the wall as

$$L_b : \begin{cases} x = f(t), \\ y = g(t), \end{cases} \qquad t \in [t_*,\ t_c]. \tag{2}$$

Concretely, the boundary (including the wall between two cells) of cell Ω_1 satisfies the following:

$$L_a \cup L_b :\ P(0) = P|_{t=0} = P(t_*) = P|_{t=t_*} \xrightarrow{L_a} P(t^*) = P|_{t=t^*} \xrightarrow{L_b} P(t_c) = P|_{t=t_c}; \tag{3}$$

and the cell Ω_2 has the boundary

$$L_b \cup L_c : P(t^*) = P|_{t=t^*} \xrightarrow{L_b} P(t_c) = P|_{t=t_c} \xrightarrow{L_c} P(T) = P|_{t=T}. \tag{4}$$

Here, it has two pairs of conjunct points

$$P(t^*) = P(T),\ P(t_*) = P(t_c)(= (0, 0) \text{ fixed it as the coordinate origin}) \tag{5}$$

and the total length

$$T = t_* + (t^* - t_*) + (t_c - t^*) + (T - t_c)(\text{ with } t_* = 0).$$

The lengths for all three curves are individually

$$|L_a| = (t^* - t_*),\ |L_b| = (t_c - t^*),\ |L_c| = (T - t_c). \tag{6}$$

And, the two cells have areas

$$|\Omega_1| = \frac{1}{2}\oint_{L_a \cup L_b} x\mathrm{d}y - y\mathrm{d}x, \text{ and } |\Omega_2| = \frac{1}{2}\oint_{(-L_b)\cup(-L_c)} x\mathrm{d}y - y\mathrm{d}x.$$

2.1. Equations for model

Based on the physical properties of cells and the mentioned analysis, we construct objective function (Lagrangian function) of variational problems with constraints as follows:

$$\widetilde{W} = \lambda_1((t^* - t_*) + (T - t_c)) + \lambda_2(t_c - t^*) + \lambda_3\left\{(|\Omega_1| - A_{01})^2 + (|\Omega_2| - A_{02})^2\right\}, \tag{7}$$

in which A_{01} and A_{02} denote the ideal areas (target areas) for two cells (domain) Ω_1 and Ω_2, respectively. Our goal is to find a group of curves $L_a \cup L_b \cup L_c$ such that the difference $\left\{(|\Omega_1| - A_{01})^2 + (|\Omega_2| - A_{02})^2\right\}$ reaches the minimum under the assumption of fixed total length T of these curves. Parameters λ_1 and λ_2 show the differentiation between the inner wall and the boundaries, they are considered as a joint expression of adhesion and contractile force on different edges.

Using λ_3 to divide the formula, one can get a simplified objective function

$$\begin{aligned} W &= W(\lambda, \mu; \varphi, \psi, f, g, p, q) \\ &= \lambda(t^* + T - t_c) + \mu(t_c - t^*) + (|\Omega_1| - A_{01})^2 + (|\Omega_2| - A_{02})^2 \\ &= \lambda\left\{\int_0^{t^*} \sqrt{\varphi'^2(t) + \psi'^2(t)}\mathrm{d}t + \int_{t_c}^{T} \sqrt{p'^2(t) + q'^2(t)}\mathrm{d}t\right\} \\ &\quad + \mu\int_{t^*}^{t_c} \sqrt{f'^2(t) + g'^2(t)}\mathrm{d}t \\ &\quad + \left\{\frac{1}{2}\left[\int_0^{t^*} (\varphi(t)\psi'(t) - \varphi'(t)\psi(t))\mathrm{d}t + \int_{t^*}^{t_c} (f(t)g'(t) - f'(t)g(t))\mathrm{d}t\right] - A_{01}\right\}^2 \\ &\quad + \left\{\frac{1}{2}\left[\int_{t^*}^{t_c} (f'(t)g(t) - f(t)g'(t))\mathrm{d}t + \int_{t_c}^{T} (p'(t)q(t) - p(t)q'(t))\mathrm{d}t\right] - A_{02}\right\}^2, \end{aligned} \tag{8}$$

in which $\lambda = \lambda_1/\lambda_3$ and $\mu = \lambda_2/\lambda_3$. The constant λ/μ is the ratio of adhesive tensions on the boundary to inner wall. From the junction condition [Eq. (5)], we have that

$$P(t^*)=P(T):\begin{cases}\varphi(t^*)=f(t^*)=p(T),\\ \psi(t^*)=g(t^*)=q(T);\end{cases} \tag{9}$$

and

$$P(t_*)=P(t_c)=(0,0):\begin{cases}\varphi(0)=f(t_c)=p(t_c)=0,\\ \psi(0)=g(t_c)=q(t_c)=0.\end{cases} \tag{10}$$

Introducing perturbation functions and their boundary value conditions

$$\begin{cases}L_a:(\varphi_1(t),\psi_1(t)), & t\in[0,\ t_*];\\ L_b:(f_1(t),g_1(t)), & t\in[t^*,\ t_c];\\ L_c:(p_1(t),q_1(t)), & t\in[t_c,\ T];\end{cases} \tag{11}$$

and

$$\begin{cases}P(0)=P(t_c):(\varphi_1(0),\psi_1(0))=(f_1(t_c),g_1(t_c))=(p_1(t_c),q_1(t_c))=(0,0),\\ P(t^*)=P(T):(\varphi_1(t^*),\psi_1(t^*))=(f_1(t^*),g_1(t^*))=(p_1(T),q_1(T)).\end{cases} \tag{12}$$

Then, Lagrangian function becomes

$$W(\varepsilon)=W(\lambda,\mu;\varphi+\varepsilon\varphi_1,\psi+\varepsilon\psi_1,f+\varepsilon f_1,g+\varepsilon g_1,p+\varepsilon p_1,q+\varepsilon q_1). \tag{13}$$

One should take notice that the constants t^* and t_c in Equations (13) and (8) depend upon the parameter ε. By discussion at the saddle point (the stationary point) $\varepsilon=0$ (see Section 5 for detailed deduction), that is, $\frac{\mathrm{d}}{\mathrm{d}\varepsilon}W(\varepsilon)|_{\varepsilon=0}=0$, one has the equations for the three curves:

$$\lambda\frac{\mathrm{d}}{\mathrm{d}t}\frac{\{\varphi',\psi'\}}{\sqrt{\varphi'^2+\psi'^2}}=C(A_{01})\{\psi',\ -\varphi'\},\qquad t\in(0,\ t^*); \tag{14a}$$

$$\mu\frac{\mathrm{d}}{\mathrm{d}t}\frac{\{f',g'\}}{\sqrt{f'^2+g'^2}}=(C(A_{01})+C(A_{02}))\{g',\ -f'\},\qquad t\in(t^*,\ t_c); \tag{14b}$$

$$\lambda\frac{\mathrm{d}}{\mathrm{d}t}\frac{\{p',q'\}}{\sqrt{p'^2+q'^2}}=C(A_{02})\{q',\ -p'\},\qquad t\in(t_c,\ T). \tag{14c}$$

In the mentioned Equation system (14), two notations are

$$\begin{aligned}&C(A_{01})\\ &=\int_0^{t^*(0)}(\varphi(t)\psi'(t)-\varphi'(t)\psi(t))\mathrm{d}t+\int_{t^*(0)}^{t_c(0)}(f(t)g'(t)-f'(t)g(t))\mathrm{d}t-2A_{01},\end{aligned} \tag{15}$$

$$\begin{aligned}&C(A_{02})\\ &=\int_{t^*(0)}^{t_c(0)}(f'(t)g(t)-f(t)g'(t))\mathrm{d}t+\int_{t_c(0)}^{T}(p'(t)q(t)-p(t)q'(t))\mathrm{d}t-2A_{02}.\end{aligned} \tag{16}$$

2.2. Boundary value conditions

Let us see the junction points $P(t_*)=P(t_c)=(0,0)$ and $P(t^*)=P(T)$, the joint point conditions for Equation system (14) are as follows:

$$\begin{aligned}&\{\varphi_1(0),\psi_1(0)\}\cdot\\ &\left[\frac{-\lambda\{\varphi'(0),\psi'(0)\}}{\sqrt{\varphi'^2(0)+\psi'^2(0)}}+\frac{\mu\{f'(t_c(0)),g'(t_c(0))\}}{\sqrt{f'^2(t_c(0))+g'^2(t_c(0))}}+\frac{-\lambda\{p'(t_c(0)),q'(t_c(0))\}}{\sqrt{p'^2(t_c(0))+q'^2(t_c(0))}}\right]\\ &+\{p_1(T),q_1(T)\}\cdot\\ &\left[\frac{\lambda\{\varphi'(t^*(0)),\psi'(t^*(0))\}}{\sqrt{\varphi'^2(t^*(0))+\psi'^2(t^*(0))}}-\frac{\mu\{f'(t^*(0)),g'(t^*(0))\}}{\sqrt{f'^2(t^*(0))+g'^2(t^*(0))}}+\frac{\lambda\{p'(T),q'(T)\}}{\sqrt{p'^2(T)+q'^2(T)}}\right]\\ &=0.\end{aligned} \tag{17}$$

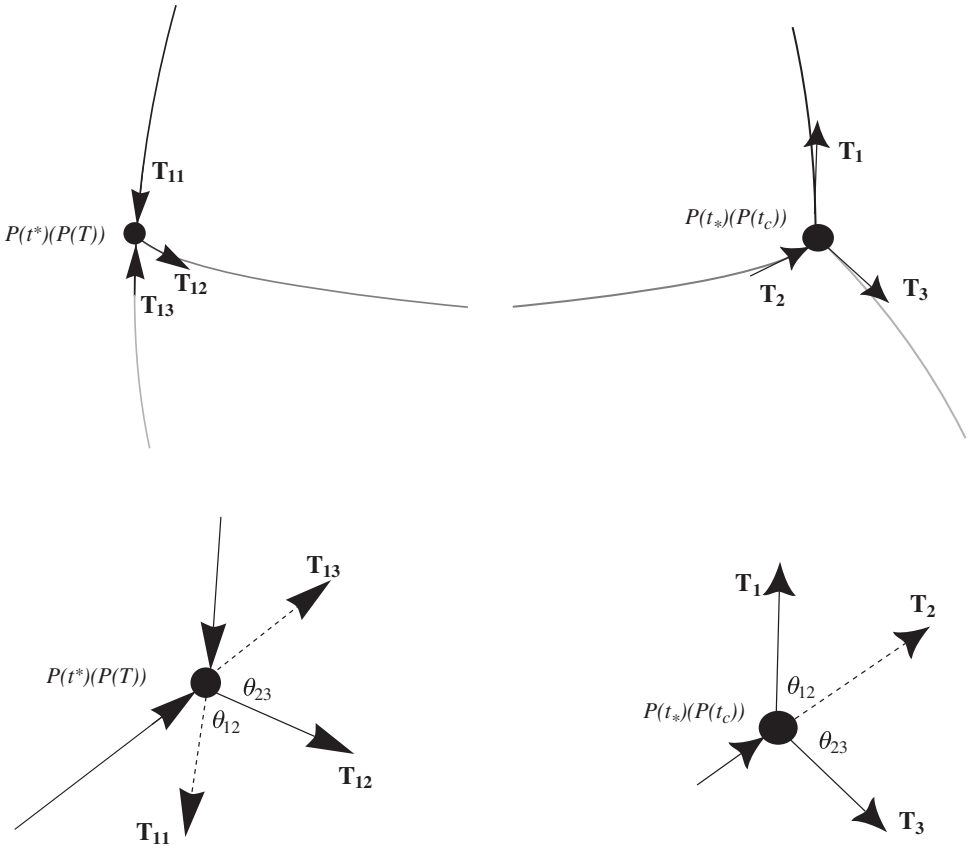

FIG. 4. The diagrammatic sketch for tangent vectors at two junction points.

By introducing the unit vectors (refer to Fig. 4)

$$\mathbf{T}_{01}=\frac{\{\varphi'(0),\psi'(0)\}}{\sqrt{\varphi'^2(0)+\psi'^2(0)}},\qquad \mathbf{T}_{11}=\frac{\{\varphi'(t^*(0)),\psi'(t^*(0))\}}{\sqrt{\varphi'^2(t^*(0))+\psi'^2(t^*(0))}},\tag{18a}$$

$$\mathbf{T}_{02}=\frac{\{f'(t_c(0)),g'(t_c(0))\}}{\sqrt{f'^2(t_c(0))+g'^2(t_c(0))}},\qquad \mathbf{T}_{12}=\frac{\{f'(t^*(0)),g'(t^*(0))\}}{\sqrt{f'^2(t^*(0))+g'^2(t^*(0))}},\tag{18b}$$

$$\mathbf{T}_{03}=\frac{\{p'(t_c(0)),q'(t_c(0))\}}{\sqrt{p'^2(t_c(0))+q'^2(t_c(0))}},\qquad \mathbf{T}_{13}=\frac{\{p'(T),q'(T)\}}{\sqrt{p'^2(T)+q'^2(T)}},\tag{18c}$$

and using the arbitrariness of the vectors $\{\varphi_1(0),\psi_1(0)\}$ and $\{p_1(T),q_1(T)\}$, the mentioned Equation (17) becomes

$$-\lambda\mathbf{T}_{01}+\mu\mathbf{T}_{02}-\lambda\mathbf{T}_{03}=0,\tag{19a}$$

$$\lambda\mathbf{T}_{11}-\mu\mathbf{T}_{12}+\lambda\mathbf{T}_{13}=0.\tag{19b}$$

Therefore, from Equations (19), we have

$$\cos\theta_{12}=\cos\theta_{23}=\langle\mathbf{T}_{01},\mathbf{T}_{02}\rangle=\langle\mathbf{T}_{11},\mathbf{T}_{12}\rangle=\langle\mathbf{T}_{02},\mathbf{T}_{03}\rangle=\langle\mathbf{T}_{12},\mathbf{T}_{13}\rangle=\frac{\mu}{2\lambda},\tag{20a}$$

$$\cos\theta_{13}=\langle\mathbf{T}_{01},\mathbf{T}_{03}\rangle=\langle\mathbf{T}_{11},\mathbf{T}_{13}\rangle=-1+\frac{\mu^2}{2\lambda^2}.\tag{20b}$$

Here, the $\langle\mathbf{T}_1,\mathbf{T}_2\rangle$ means the inner product of two vectors $\mathbf{T}_1$ and $\mathbf{T}_2$. And θ_{ij} denotes the intersection angle between two vectors $\mathbf{T}_{li}$ and $\mathbf{T}_{lj}$ ($i,j=1,2,3$; and $l=0,1$).

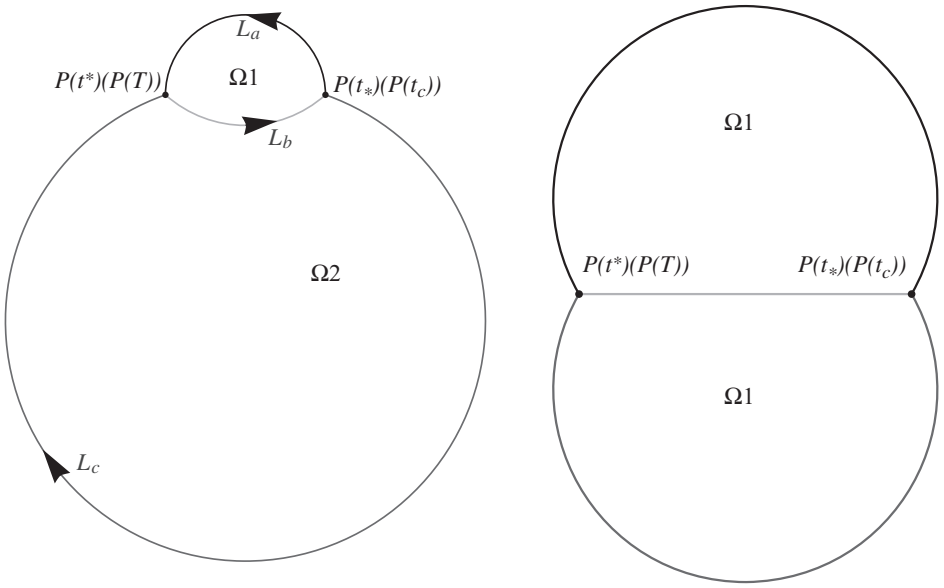

FIG. 5. Effect of sizes on the shape of colony with equal weight (all adhesive tensions on boundaries and wall at each junction are equal). Two cells have equal size in the right side figure.

Now let us summarize the previous discussion.

Theorem 1. *A colony of two cells satisfies a weighted bubble model, and its edges comply with the following boundary value problem:*

$$\textit{the outer boundary } L_{o1}: \lambda \frac{\mathrm{d}}{\mathrm{d}t} \frac{\{\varphi', \psi'\}}{\sqrt{\varphi'^2 + \psi'^2}} = \kappa_1 \{\psi', -\varphi'\}, \qquad t \in (0,\ t^*); \tag{21a}$$

$$\textit{the inner wall } L_{iw}: \mu \frac{\mathrm{d}}{\mathrm{d}t} \frac{\{f', g'\}}{\sqrt{f'^2 + g'^2}} = (\kappa_1 + \kappa_2)\{g', -f'\}, \qquad t \in (t^*,\ t_c); \tag{21b}$$

$$\textit{the outer boundary } L_{o2}: \lambda \frac{\mathrm{d}}{\mathrm{d}t} \frac{\{p', q'\}}{\sqrt{p'^2 + q'^2}} = \kappa_2 \{q', -p'\}, \qquad t \in (t_c,\ T) \tag{21c}$$

with the boundary condition on junctions that the inner wall L_{iw} is on the angular bisector of the angle 2θ between two outer boundaries L_{o1} and L_{o2}, and $\cos\theta = \frac{\mu}{2\lambda}$.

One can find from Equations (20) for positive constants λ and μ that the two tangent vectors $\mathbf{T}_{01}$ and $\mathbf{T}_{03}$ starting from $P(0) = P(t_c)$ have an acute angle θ_{13}, and that the tangent vector $\mathbf{T}_{01}$ has an obtuse angle with the tangent vector θ_{02} pointing to $P(t_c)$. The two outer boundaries have the same angle with the inner wall, that is, the tangent vector of the inner wall is on the angular bisector of the intersection angle of the boundaries, $\theta_{13} = 2\theta_{12} = 2\theta_{23}$ (refer to Fig. 4).

Particularly, Equations (20) show that the three tangents have an equal intersection angle $2\pi/3$ at each junction (Fig. 5).

Turn to the means for the parameters λ and μ [refer to Eqs. (7) and (8)], we assume that the colony of C cells is around P cells (refer to Käfer et al., 2007; Gemp et al., 2011 for discussion on the compound eye of *Drosophila*). If C-C tension coefficient μ (on the wall), mediated by both E- and N-cadherin, is weaker than C-P tension (on the boundaries), λ, which are mediated by E-cadherin alone, that is, $\lambda > \mu$, then the angle $\theta = \theta_{12} = \arccos\frac{\mu}{2\lambda} \to \pi/2$ (so, the intersection angle between two outer boundaries becomes π as $\mu \to 0+$). On the contrary, θ becomes zero as μ increases to 2λ.

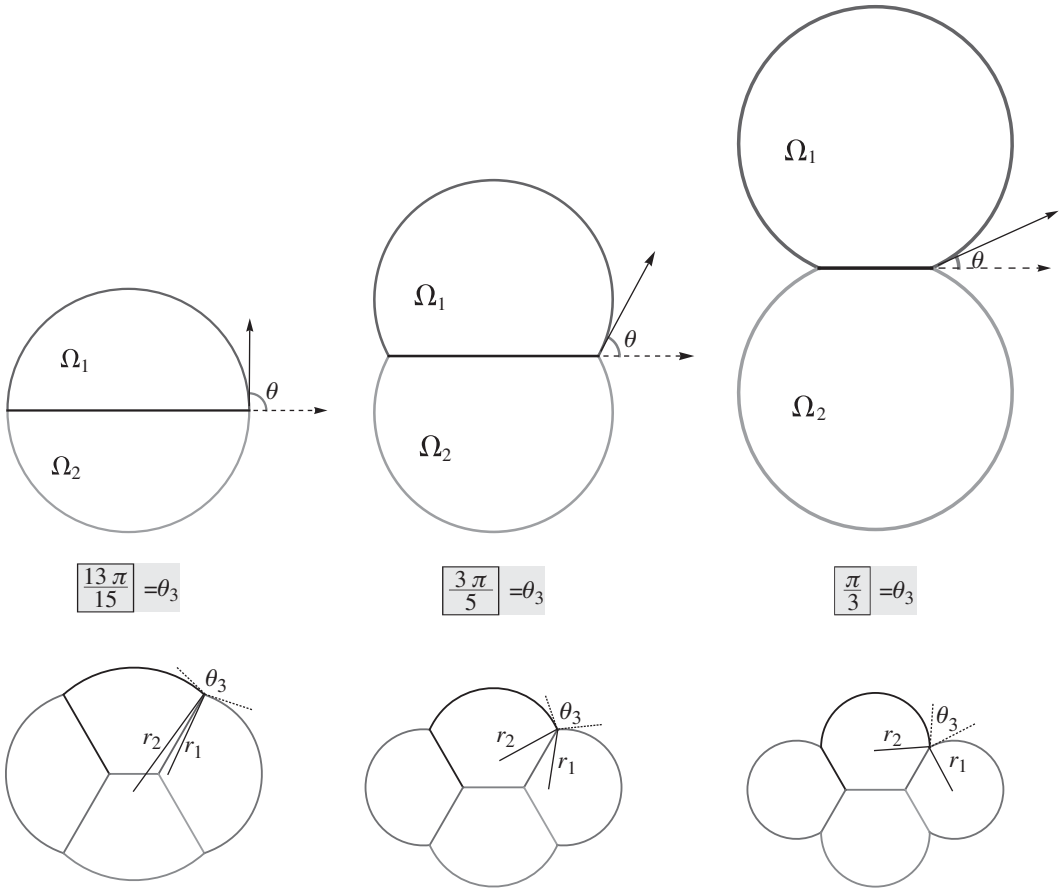

FIG. 6. Effect of tension on the pattern of cell colony. The top line represents 2-bubble cells, the lower line represents 4-bubble cells. The tension on the inner wall(s) decreases from the left to the right.

3. SIMULATION

The 2-bubble model shows in the first line of Figure 6 the pattern varies with the change in tension. The adhesive tension on the wall in the first image is bigger than that of the second image, and so on.

To simulate the 4-bubble model (Fig. 6), we assume that every cell in the colony has the same area π, the radii for the right cell and the upper cell are denoted by r_1 and r_2, respectively. Let

$$\Phi_1(\theta) := \sqrt{5\pi - 6\theta + 4\sqrt{3}\cos\theta\ \sin\left(\frac{\pi}{6}+\theta\right)};$$

$$\Phi_2(\theta) := (2\pi - 3\theta)\sec^2(\pi/6-\theta) + 3\tan\left(\frac{\pi}{6}-\theta\right);$$

$$\Phi_3(\theta) := \frac{3(3\sqrt{3}\cos\theta + 2(5\pi-6\theta)\cos(\pi/3+\theta) + \sqrt{3}\cos(3\theta) + 12\cos^2\theta\sin\theta)}{2\sin(\pi/3+\theta)};$$

$$\Phi(\theta) := \frac{1}{\Phi_1(\theta)}\sqrt{\Phi_3(\theta) + (2\pi-3\theta)\left({\Phi_1}^2(\theta) + 2\sqrt{3}\sin^2\left(\frac{\pi}{6}+\theta\right)\right)\sec^2\left(\frac{\pi}{6}-\theta\right)};$$

$$s(\theta) := \frac{\sqrt{\pi}}{\Phi_1(\theta)\Phi_2(\theta)}\left[\left(\sqrt{2}(3\theta-2\pi)\sec^2\left(\frac{\pi}{6}-\theta\right) - 3\sqrt{6}\right)\sin\left(\frac{\pi}{6}+\theta\right)\right.$$

$$\left. + \sqrt{3}\Phi_1(\theta)\Phi(\theta) - 3\sqrt{2}\sin\left(\frac{\pi}{6}+\theta\right)\tan\left(\frac{\pi}{6}-\theta\right)\right].$$

And, let

$$\theta_s(\theta) := \pi/2-\theta;$$
$$r_1(\theta) := \frac{\sqrt{6\pi}}{\sqrt{5\pi-6\theta+4\sqrt{3}\cos\theta\cdot\sin(\pi/6+\theta)}},$$
$$\theta_1(\theta) := 2(5\pi/6-\theta)\ (\text{the central angle of the right cell}),$$
$$x_1(\theta) := s(\theta)+\frac{2\sqrt{2\pi}\cos\theta}{\sqrt{5\pi-6\theta+4\sqrt{3}\cos\theta\cdot\sin(\pi/6+\theta)}};$$
$$\rho(\theta) := \frac{2r_1(\theta)}{\sqrt{3}}\sin(2\pi/3-\theta_s(\theta)).$$

Then, the area of the right cell is

$$S_r=\frac{1}{2}{r_1}^2\cdot 2(\theta_s+\pi/3)+2\cdot\frac{1}{2}\rho\sin\frac{\pi}{3}\cdot(x_1-s),$$

in which the center of the right cell is $(x_1(\theta), 0)$. And, the area of the upper cell is

$$S_u=\frac{1}{2}r_2^2\theta_2+2\cdot\frac{1}{2}\left(y_2+\rho\sin\frac{\pi}{3}\right)\left(s+\rho\sin\frac{\pi}{3}\right)-2\cdot\frac{1}{2}\rho\cos\frac{\pi}{3}\sin\frac{\pi}{3},$$

in which the center is $(0, y_2(\theta))$ with

$$y_2(\theta)=\frac{\sqrt{3\pi}}{\Phi_1(\theta)\Phi_2(\theta)}\left[\sqrt{2}(2\pi-3\theta)\sec^2\left(\frac{\pi}{6}-\theta\right)\sin\left(\frac{\pi}{6}+\theta\right)+\Phi_1(\theta)\Phi(\theta)\tan\left(\frac{\pi}{6}-\theta\right)\right],$$

and

$$\theta_2(\theta)=4\pi/3-2\theta\ (\text{the central angle of the upper cell}),$$
$$r_2(\theta)=\frac{\sqrt{3\pi}\sec\left(\frac{\pi}{6}-\theta\right)\left(\Phi_1(\theta)\Phi(\theta)-3\sqrt{2}\sin\left(\frac{\pi}{6}+\theta\right)\right)}{\Phi_1(\theta)\left((2\pi-3\theta)\sec^2\left(\frac{\pi}{6}-\theta\right)+3\tan\left(\frac{\pi}{6}-\theta\right)\right)}.$$

For a colony of *Pediastrum* (e.g., *Pediastrum boryanum*) or *Tetrastrum* Chodat, the difference between the walls and the boundaries can be described as for cells of *Drosophila*, just the prongs on the boundaries should be noticed.

As an extreme (limit) case, $\lambda \gg \mu$, the division of *Coleochaete* cells can be thought as a connection with this case, especially, for the initial division from one to two cells (e.g., refer to Besson and Dumais, 2011; Wang and Cong, 2015). A division for a disk with area 4π by using two vertical diameters has a total length (circumference and two diameters) $l_d = 8+4\pi \doteq 20.5664$ being bigger than that of the 4-bubble model

$$l_{\text{total}}=\frac{18\left(\sqrt{3}-3\right)\pi+8\sqrt{3}\pi^2+(2\pi+3)\sqrt{6\pi\left(4\pi-3\sqrt{3}\right)}-108}{6\pi-9\sqrt{3}}\doteq 20.384$$

as the case of the first image in the second line in Figure 6 (where $r_2=\frac{9-\sqrt{3\left(8\pi^2-6\sqrt{3}\pi\right)}}{3\sqrt{3}-2\pi}\doteq 2.56355$).

4. DISCUSSION

In this study, we investigated the bubble model with weights for a colony of cells. Variational method is critical for the model establishment. As a simple case, 2-bubble cell model with weights is investigated in detail, this method can be used to consider 3-bubble cell model. Hayashi and Carthew (2004) introduced this cell model, but have not given consideration to the difference among different edges of tensions and the consequences. For a more complex bubble model, such as *N*-bubble model ($N \geq 4$), the existence and the solvability ''remain unproven'' (Morgan, 2009). Hence, a general case for weighted edges has no result yet.

This article discusses the issue with weight, especially on the theoretical analysis on the construction of differential model. The result given shows that all edges (the outer boundaries and the inner walls) are arcs with different curvatures, and that accompanies the angles of the three tangent lines at the junction points

determined by the weights on edges. These weights describe the adhesive tensions that vary according to the different edges of the cells. Based on analysis of angle data, we think that this model is more suitable to describe the shape character of a cone cell group in *Drosophila* retina. The distribution of the outer angles is closer to Gaussian, and the average is 147.73° for experimental data in Chan et al. (2017). However, this average is different from the analytical results of Hilgenfeldt et al. (2008), in which experimental values are in $(130°-9°, 130°+9°)$, an simulation value for their model is 128°.

We also use it to explain the formation of green algae cells such as *Pediastrum* and *Tetrastrum* (refer to Section 6). Flagella of these two kinds of cells of green algae have a great influence on the shape of the outer boundary of cells. Although the direct result of this influence is also reflected in the wide range of these angular distributions, the data show that they obey the normal distribution (Gaussian).

Our results demonstrate mathematically how the pattern of a colony of cells can render the role of adhesive tension in a developing biological structure. We suggest that the relationships between adhesion and colony pattern might contribute to the diversity of patterns seen in Chlorophyta.

5. APPENDIX A1: DERIVATION ON CELL MODEL

We discuss how to get Equations (14) and its boundary value condition Equation (17). Let us substitute Equations (11) into Lagrangian function Equation (13), it has

$$
\begin{aligned}
W(\varepsilon) &= W(\lambda, \mu; \varphi+\varepsilon\varphi_1, \psi+\varepsilon\psi_1, f+\varepsilon f_1, g+\varepsilon g_1, p+\varepsilon p_1, q+\varepsilon q_1)\\
&= \lambda\left\{\int_0^{t^*(\varepsilon)} \sqrt{(\varphi'(t)+\varepsilon\varphi'_1(t))^2+(\psi'(t)+\varepsilon\psi'_1(t))^2}\,\mathrm{d}t\right.\\
&\left.+\int_{t_c(\varepsilon)}^{T} \sqrt{(p'(t)+\varepsilon p'_1(t))^2+(q'(t)+\varepsilon q'_1(t))^2}\,\mathrm{d}t\right\}\\
&+\mu\int_{t^*(\varepsilon)}^{t_c(\varepsilon)} \sqrt{(f'(t)+\varepsilon f'_1(t))^2+(g'(t)+\varepsilon g'_1(t))^2}\,\mathrm{d}t\\
&+\left\{\frac{1}{2}\left[\int_0^{t^*(\varepsilon)}((\varphi(t)+\varepsilon\varphi_1(t))(\psi'(t)+\varepsilon\psi'_1(t))-(\varphi'(t)+\varepsilon\varphi'_1(t))(\psi(t)+\varepsilon\psi_1(t)))\mathrm{d}t\right.\right.\\
&\left.\left.+\int_{t^*(\varepsilon)}^{t_c(\varepsilon)}((f(t)+\varepsilon f_1(t))(g'(t)+\varepsilon g'_1(t))-(f'(t)+\varepsilon f'_1(t))(g(t)+\varepsilon g_1(t)))\mathrm{d}t\right]-A_{01}\right\}^2\\
&+\left\{\frac{1}{2}\left[\int_{t^*(\varepsilon)}^{t_c(\varepsilon)}((f'(t)+\varepsilon f'_1(t))(g(t)+\varepsilon g_1(t))-(f(t)+\varepsilon f_1(t))(g'(t)+\varepsilon g'_1(t)))\mathrm{d}t\right.\right.\\
&\left.\left.+\int_{t_c(\varepsilon)}^{T}((p'(t)+\varepsilon p'_1(t))(q(t)+\varepsilon q_1(t))-(p(t)+\varepsilon p_1(t))(q'(t)+\varepsilon q'_1(t)))\mathrm{d}t\right]-A_{02}\right\}^2.
\end{aligned}
\tag{22}
$$

The first derivative of W with respect to ε is

$$
\begin{aligned}
\frac{\mathrm{d}}{\mathrm{d}\varepsilon}W(\varepsilon) = \lambda\Bigg\{&\int_0^{t^*(\varepsilon)}\frac{2((\varphi'+\varepsilon\varphi'_1)\varphi'_1+(\psi'+\varepsilon\psi'_1)\psi'_1)}{2\sqrt{(\varphi'+\varepsilon\varphi'_1)^2+(\psi'+\varepsilon\psi'_1)^2}}\mathrm{d}t\\
&+\sqrt{(\varphi'+\varepsilon\varphi'_1)^2+(\psi'+\varepsilon\psi'_1)^2}\big|_{t=t^*(\varepsilon)}\cdot\frac{\mathrm{d}t^*(\varepsilon)}{\mathrm{d}\varepsilon}\\
&+\int_{t_c(\varepsilon)}^{T}\frac{2((p'+\varepsilon p'_1)p'_1+(q'+\varepsilon q'_1)q'_1)}{2\sqrt{(p'+\varepsilon p'_1)^2+(q'+\varepsilon q'_1)^2}}\mathrm{d}t\\
&-\sqrt{(p'+\varepsilon p'_1)^2+(q'+\varepsilon q'_1)^2}\big|_{t=t_c(\varepsilon)}\cdot\frac{\mathrm{d}t_c(\varepsilon)}{\mathrm{d}\varepsilon}\Bigg\}\\
&+\mu\left\{\int_{t^*(\varepsilon)}^{t_c(\varepsilon)}\frac{2((f'+\varepsilon f'_1)f'_1+(g'+\varepsilon g'_1)g'_1)}{2\sqrt{(f'+\varepsilon f'_1)^2+(g'+\varepsilon g'_1)^2}}\mathrm{d}t\right.
\end{aligned}
$$

$$+\sqrt{(f'+\varepsilon f'_1)^2+(g'+\varepsilon g'_1)^2}|_{t=t_c(\varepsilon)}\cdot\frac{\mathrm{d}t_c(\varepsilon)}{\mathrm{d}\varepsilon}$$
$$-\sqrt{(f'+\varepsilon f'_1)^2+(g'+\varepsilon g'_1)^2}|_{t=t^*(\varepsilon)}\cdot\frac{\mathrm{d}t^*(\varepsilon)}{\mathrm{d}\varepsilon}\Bigg\}$$
$$+\Bigg[\int_0^{t^*(\varepsilon)}\Big((\varphi(t)+\varepsilon\varphi_1(t))(\psi'(t)+\varepsilon\psi'_1(t))-(\varphi'(t)+\varepsilon\varphi'_1(t))(\psi(t)+\varepsilon\psi_1(t))\Big)\mathrm{d}t$$
$$+\int_{t^*(\varepsilon)}^{t_c(\varepsilon)}\Big((f(t)+\varepsilon f_1(t))(g'(t)+\varepsilon g'_1(t))-(f'(t)+\varepsilon f'_1(t))(g(t)+\varepsilon g_1(t))\Big)\mathrm{d}t-2A_{01}\Bigg]$$
$$\cdot\frac{1}{2}\Bigg[\int_0^{t^*(\varepsilon)}(\varphi\psi'_1+\varphi_1\psi'+2\varepsilon\varphi_1\psi'_1-\varphi'\psi_1-\varphi'_1\psi(t)-2\varepsilon\varphi'_1\psi_1)\mathrm{d}t$$
$$+\int_{t^*(\varepsilon)}^{t_c(\varepsilon)}(fg'_1+f_1g'+2\varepsilon f_1g_1{}'-f'g_1-f'_1g-2\varepsilon f'_1g_1)\mathrm{d}t$$
$$+((\varphi+\varepsilon\varphi_1)(\psi'+\varepsilon\psi'_1)-(\varphi'+\varepsilon\varphi'_1)(\psi+\varepsilon\psi_1))|_{t=t^*(\varepsilon)}\cdot\frac{\mathrm{d}t^*(\varepsilon)}{\mathrm{d}\varepsilon}$$
$$+((f+\varepsilon f_1)(g'+\varepsilon g'_1)-(f'+\varepsilon f'_1)(g+\varepsilon g_1)|_{t_c(\varepsilon)}\cdot\frac{\mathrm{d}t_c(\varepsilon)}{\mathrm{d}\varepsilon}$$
$$-((f+\varepsilon f_1)(g'+\varepsilon g'_1)-(f'+\varepsilon f'_1)(g+\varepsilon g_1)|_{t=t^*(\varepsilon)}\cdot\frac{\mathrm{d}t^*(\varepsilon)}{\mathrm{d}\varepsilon}\Bigg]$$
$$+\Bigg[\int_{t^*(\varepsilon)}^{t_c(\varepsilon)}((f'(t)+\varepsilon f'_1(t))(g(t)+\varepsilon g_1(t))-(f(t)+\varepsilon f_1(t))(g'(t)+\varepsilon g'_1(t)))\mathrm{d}t$$
$$+\int_{t_c(\varepsilon)}^{T}((p'(t)+\varepsilon p'_1(t))(q(t)+\varepsilon q_1(t))-(p(t)+\varepsilon p_1(t))(q'(t)+\varepsilon q'_1(t)))\mathrm{d}t-2A_{02}\Bigg]$$
$$\cdot\frac{1}{2}\Bigg[\int_{t^*(\varepsilon)}^{t_c(\varepsilon)}(f'g_1+f'_1g+2\varepsilon f'_1\psi_1-fg'_1-f_1g'-2\varepsilon f_1g'_1)\mathrm{d}t$$
$$+\int_{t_c(\varepsilon)}^{T}(p'q_1+p'_1q+2\varepsilon p'_1q-pq'_1-p_1q'-2\varepsilon p_1g'_1)\mathrm{d}t$$
$$+((f'+\varepsilon f'_1)(g+\varepsilon g_1)-(f+\varepsilon f_1)(g'+\varepsilon g'_1))|_{t=t_c(\varepsilon)}\cdot\frac{\mathrm{d}t_c(\varepsilon)}{\mathrm{d}\varepsilon}$$
$$-((f'+\varepsilon f'_1)(g+\varepsilon g_1)-(f+\varepsilon f_1)(g'+\varepsilon g'_1))|_{t=t^*(\varepsilon)}\cdot\frac{\mathrm{d}t^*(\varepsilon)}{\mathrm{d}\varepsilon}$$
$$-((p'+\varepsilon p'_1)(q+\varepsilon q_1)-(p+\varepsilon p_1)(q'+\varepsilon q'_1))|_{t=t_c(\varepsilon)}\cdot\frac{\mathrm{d}t_c(\varepsilon)}{\mathrm{d}\varepsilon}\Bigg].$$

It is the saddle point as $\varepsilon=0$, that is,

$$\frac{\mathrm{d}}{\mathrm{d}\varepsilon}W(\varepsilon)|_{\varepsilon=0}=\lambda\Bigg\{\int_0^{t^*(0)}\frac{\varphi'\varphi'_1+\psi'\psi'_1}{\sqrt{\varphi'^2+\psi'^2}}\mathrm{d}t+\int_{t_c(0)}^{T}\frac{p'p'_1+q'q'_1}{\sqrt{p'^2+q'^2}}\mathrm{d}t$$
$$+\sqrt{\varphi'^2+\psi'^2}|_{t=t^*(0)}\cdot\frac{\mathrm{d}t^*(\varepsilon)}{\mathrm{d}\varepsilon}|_{\varepsilon=0}-\sqrt{p'^2+q'^2}|_{t=t_c(0)}\cdot\frac{\mathrm{d}t_c(\varepsilon)}{\mathrm{d}\varepsilon}|_{\varepsilon=0}\Bigg\}$$
$$+\mu\Bigg\{\int_{t^*(0)}^{t_c(0)}\frac{f'f'_1+g'g'_1}{\sqrt{f'^2+g'^2}}\mathrm{d}t+\sqrt{f'^2+g'^2}|_{t=t_c(0)}\cdot\frac{\mathrm{d}t_c(\varepsilon)}{\mathrm{d}\varepsilon}|_{\varepsilon=0}$$
$$-\sqrt{f'^2+g'^2}|_{t=t^*(0)}\cdot\frac{\mathrm{d}t^*(\varepsilon)}{\mathrm{d}\varepsilon}|_{\varepsilon=0}\Bigg\}$$

$$+\left[\int_0^{t^*(0)}(\varphi(t)\psi'(t)-\varphi'(t)\psi(t))\mathrm{d}t+\int_{t^*(0)}^{t_c(0)}(f(t)g'(t)-f'(t)g(t))\mathrm{d}t-2A_{01}\right]$$
$$\cdot\frac{1}{2}\left[\int_0^{t^*(0)}(\varphi\psi_1{}'+\varphi_1\psi'-\varphi'\psi_1-\varphi'_1\psi(t))\mathrm{d}t\right.$$
$$+\int_{t^*(0)}^{t_c(0)}(fg'_1+f_1g'-f'g_1-f'_1g)\mathrm{d}t$$
$$+(\varphi\psi'-\varphi'\psi)|_{t=t^*(0)}\cdot\frac{\mathrm{d}t^*(\varepsilon)}{\mathrm{d}\varepsilon}|_{\varepsilon=0}+(fg'-f'g)|_{t_c(0)}\cdot\frac{\mathrm{d}t_c(\varepsilon)}{\mathrm{d}\varepsilon}|_{\varepsilon=0}$$
$$\left.-(fg'-f'g)|_{t=t^*(0)}\cdot\frac{\mathrm{d}t^*(\varepsilon)}{\mathrm{d}\varepsilon}|_{\varepsilon=0}\right]$$
$$+\left[\int_{t^*(0)}^{t_c(0)}(f'(t)g(t)-f(t)g'(t))\mathrm{d}t+\int_{t_c(0)}^{T}(p'(t)q(t)-p(t)q'(t))\mathrm{d}t-2A_{02}\right]$$
$$\cdot\frac{1}{2}\left[\int_{t^*(0)}^{t_c(0)}(f'g_1+f'_1g-fg'_1-f_1g')\mathrm{d}t\right.$$
$$+\int_{t_c(0)}^{T}(p'q_1+p'_1q-pq'_1-p_1q')\mathrm{d}t$$
$$+(f'g-fg'))|_{t=t_c(0)}\cdot\frac{\mathrm{d}t_c(\varepsilon)}{\mathrm{d}\varepsilon}|_{\varepsilon=0}-(f'g-fg')|_{t=t^*(0)}\cdot\frac{\mathrm{d}t^*(\varepsilon)}{\mathrm{d}\varepsilon}|_{\varepsilon=0}$$
$$\left.-(p'q-pq')|_{t=t_c(0)}\cdot\frac{\mathrm{d}t_c(\varepsilon)}{\mathrm{d}\varepsilon}|_{\varepsilon=0}\right].$$

Taking integration by parts, then it follows that

$$\frac{\mathrm{d}}{\mathrm{d}\varepsilon}W(\varepsilon)|_{\varepsilon=0}=\lambda\left\{\frac{\varphi'\varphi_1+\psi'\psi_1}{\sqrt{\varphi'^2+\psi'^2}}|_{t=0}^{t=t^*(0)}+\frac{p'p_1+q'q_1}{\sqrt{p'^2+q'^2}}|_{t=t_c(0)}^{t=T}\right.$$
$$-\int_0^{t^*(0)}\{\varphi_1,\psi_1\}\cdot\frac{\mathrm{d}}{\mathrm{d}t}\frac{\{\varphi',\psi'\}}{\sqrt{\varphi'^2+\psi'^2}}\mathrm{d}t-\int_{t_c(0)}^{T}\{p_1,q_1\}\cdot\frac{\mathrm{d}}{\mathrm{d}t}\frac{\{p',q'\}}{\sqrt{p'^2+q'^2}}\mathrm{d}t$$
$$\left.+\sqrt{\varphi'^2+\psi'^2}|_{t=t^*(0)}\cdot\frac{\mathrm{d}t^*(\varepsilon)}{\mathrm{d}\varepsilon}|_{\varepsilon=0}-\sqrt{p'^2+q'^2}|_{t=t_c(0)}\cdot\frac{\mathrm{d}t_c(\varepsilon)}{\mathrm{d}\varepsilon}|_{\varepsilon=0}\right\}$$
$$+\mu\left\{\frac{f'f_1+g'g_1}{\sqrt{f'^2+g'^2}}|_{t=t^*(0)}^{t=t_c(0)}-\int_{t^*(0)}^{t_c(0)}\{f_1,g_1\}\cdot\frac{\mathrm{d}}{\mathrm{d}t}\frac{\{f',g'\}}{\sqrt{f'^2+g'^2}}\mathrm{d}t\right.$$
$$\left.+\sqrt{f'^2+g'^2}|_{t=t_c(0)}\cdot\frac{\mathrm{d}t_c(\varepsilon)}{\mathrm{d}\varepsilon}|_{\varepsilon=0}-\sqrt{f'^2+g'^2}|_{t=t^*(0)}\cdot\frac{\mathrm{d}t^*(\varepsilon)}{\mathrm{d}\varepsilon}|_{\varepsilon=0}\right\}$$
$$+\left[\int_0^{t^*(0)}(\varphi(t)\psi'(t)-\varphi'(t)\psi(t))\mathrm{d}t+\int_{t^*(0)}^{t_c(0)}(f(t)g'(t)-f'(t)g(t))\mathrm{d}t-2A_{01}\right]$$
$$\cdot\frac{1}{2}\left[(\varphi\psi_1-\varphi_1\psi)|_{t=0}^{t=t^*(0)}+\int_0^{t^*(0)}(2\varphi_1\psi'-2\varphi'\psi_1)\mathrm{d}t\right.$$
$$+(fg_1-f_1g)|_{t^*(0)}^{t_c(0)}+\int_{t^*(0)}^{t_c(0)}(2f_1g'-2f'g_1)\mathrm{d}t$$
$$+(\varphi\psi'-\varphi'\psi)|_{t=t^*(0)}\cdot\frac{\mathrm{d}t^*(\varepsilon)}{\mathrm{d}\varepsilon}|_{\varepsilon=0}+(fg'-f'g)|_{t_c(0)}\cdot\frac{\mathrm{d}t_c(\varepsilon)}{\mathrm{d}\varepsilon}|_{\varepsilon=0}$$
$$\left.-(fg'-f'g)|_{t=t^*(0)}\cdot\frac{\mathrm{d}t^*(\varepsilon)}{\mathrm{d}\varepsilon}|_{\varepsilon=0}\right]$$

$$+\left[\int_{t^*(0)}^{t_c(0)}(f'(t)g(t)-f(t)g'(t))\mathrm{d}t+\int_{t_c(0)}^{T}(p'(t)q(t)-p(t)q'(t))\mathrm{d}t-2A_{02}\right]$$
$$\cdot\frac{1}{2}\left[(f_1g-fg_1)|_{t^*(0)}^{t_c(0)}-\int_{t^*(0)}^{t_c(0)}(2f'g_1-2f_1g')\mathrm{d}t\right.$$
$$+(p_1q-pq_1)|_{t_c(0)}^{T}-\int_{t_c(0)}^{T}(2p'q_1-2p_1q')\mathrm{d}t$$
$$+(f'g-fg'))|_{t=t_c(0)}\cdot\frac{\mathrm{d}t_c(\varepsilon)}{\mathrm{d}\varepsilon}|_{\varepsilon=0}-(f'g-fg')|_{t=t^*(0)}\cdot\frac{\mathrm{d}t^*(\varepsilon)}{\mathrm{d}\varepsilon}|_{\varepsilon=0}$$
$$\left.-(p'q-pq')|_{t=t_c(0)}\cdot\frac{\mathrm{d}t_c(\varepsilon)}{\mathrm{d}\varepsilon}|_{\varepsilon=0}\right].$$

Now we study the terms with integrals and with junctions separately. First, let us see the term with integrals:

$$0=\lambda\left\{-\int_0^{t^*(0)}\{\varphi_1,\psi_1\}\cdot\frac{\mathrm{d}}{\mathrm{d}t}\frac{\{\varphi',\psi'\}}{\sqrt{\varphi'^2+\psi'^2}}\mathrm{d}t-\int_{t_c(0)}^{T}\{p_1,q_1\}\cdot\frac{\mathrm{d}}{\mathrm{d}t}\frac{\{p',q'\}}{\sqrt{p'^2+q'^2}}\mathrm{d}t\right\}$$
$$+\mu\left\{-\int_{t^*(0)}^{t_c(0)}\{f_1,g_1\}\cdot\frac{\mathrm{d}}{\mathrm{d}t}\frac{\{f',g'\}}{\sqrt{f'^2+g'^2}}\mathrm{d}t\right\}$$
$$+\left[\int_0^{t^*(0)}(\varphi(t)\psi'(t)-\varphi'(t)\psi(t))\mathrm{d}t+\int_{t^*(0)}^{t_c(0)}(f(t)g'(t)-f'(t)g(t))\mathrm{d}t-2A_{01}\right]$$
$$\cdot\frac{1}{2}\left[\int_0^{t^*(0)}(2\varphi_1\psi'-2\varphi'\psi_1)\mathrm{d}t+\int_{t^*(0)}^{t_c(0)}(2f_1g'-2f'g_1)\mathrm{d}t\right]$$
$$+\left[\int_{t^*(0)}^{t_c(0)}(f'(t)g(t)-f(t)g'(t))\mathrm{d}t+\int_{t_c(0)}^{T}(p'(t)q(t)-p(t)q'(t))\mathrm{d}t-2A_{02}\right]$$
$$\cdot\frac{1}{2}\left[-\int_{t^*(0)}^{t_c(0)}(2f'g_1-2f_1g')\mathrm{d}t-\int_{t_c(0)}^{T}(2p'q_1-2p_1q')\mathrm{d}t\right]. \tag{23}$$

By using the notations

$$C(A_{01})$$
$$=\int_0^{t^*(0)}(\varphi(t)\psi'(t)-\varphi'(t)\psi(t))\mathrm{d}t+\int_{t^*(0)}^{t_c(0)}(f(t)g'(t)-f'(t)g(t))\mathrm{d}t-2A_{01}, \tag{24}$$
$$C(A_{02})$$
$$=\int_{t^*(0)}^{t_c(0)}(f'(t)g(t)-f(t)g'(t))\mathrm{d}t+\int_{t_c(0)}^{T}(p'(t)q(t)-p(t)q'(t))\mathrm{d}t-2A_{02}; \tag{25}$$

the term with integrals Equation (23) becomes

$$0=\lambda\left\{-\int_0^{t^*(0)}\{\varphi_1,\psi_1\}\cdot\frac{\mathrm{d}}{\mathrm{d}t}\frac{\{\varphi',\psi'\}}{\sqrt{\varphi'^2+\psi'^2}}\mathrm{d}t-\int_{t_c(0)}^{T}\{p_1,q_1\}\cdot\frac{\mathrm{d}}{\mathrm{d}t}\frac{\{p',q'\}}{\sqrt{p'^2+q'^2}}\mathrm{d}t\right\}$$
$$+\mu\left\{-\int_{t^*(0)}^{t_c(0)}\{f_1,g_1\}\cdot\frac{\mathrm{d}}{\mathrm{d}t}\frac{\{f',g'\}}{\sqrt{f'^2+g'^2}}\mathrm{d}t\right\}$$

$$
\begin{aligned}
&+C(A_{01})\cdot\left[\int_0^{t^*(0)}(\varphi_1\psi'-\varphi'\psi_1)\mathrm{d}t+\int_{t^*(0)}^{t_c(0)}(f_1g'-f'g_1)\mathrm{d}t\right]\\
&+C(A_{02})\cdot\left[-\int_{t^*(0)}^{t_c(0)}(f'g_1-f_1g')\mathrm{d}t-\int_{t_c(0)}^{T}(p'q_1-p_1q')\mathrm{d}t\right]\\
&=\int_0^{t^*(0)}\{\varphi_1,\psi_1\}\cdot\left[C(A_{01})\{\psi',-\varphi'\}-\lambda\frac{\mathrm{d}}{\mathrm{d}t}\frac{\{\varphi',\psi'\}}{\sqrt{\varphi'^2+\psi'^2}}\right]\mathrm{d}t\\
&+\int_{t_c(0)}^{T}\{p_1,q_1\}\cdot\left[C(A_{02})\{q',-p'\}-\lambda\frac{\mathrm{d}}{\mathrm{d}t}\frac{\{p',q'\}}{\sqrt{p'^2+q'^2}}\right]\mathrm{d}t\\
&+\int_{t^*(0)}^{t_c(0)}\{f_1,g_1\}\cdot\left[(C(A_{01})+C(A_{02}))\{g',-f'\}-\mu\frac{\mathrm{d}}{\mathrm{d}t}\frac{\{f',g'\}}{\sqrt{f'^2+g'^2}}\right]\mathrm{d}t. \qquad (26)
\end{aligned}
$$

The arbitrary of the perturbation functions implies Equation (14), that is,

$$\lambda\frac{\mathrm{d}}{\mathrm{d}t}\frac{\{\varphi',\psi'\}}{\sqrt{\varphi'^2+\psi'^2}}=C(A_{01})\{\psi',-\varphi'\},\qquad t\in(0,t^*); \qquad (27a)$$

$$\mu\frac{\mathrm{d}}{\mathrm{d}t}\frac{\{f',g'\}}{\sqrt{f'^2+g'^2}}=(C(A_{01})+C(A_{02}))\{g',-f'\},\qquad t\in(t^*,t_c); \qquad (27b)$$

$$\lambda\frac{\mathrm{d}}{\mathrm{d}t}\frac{\{p',q'\}}{\sqrt{p'^2+q'^2}}=C(A_{02})\{q',-p'\},\qquad t\in(t_c,T). \qquad (27c)$$

If $\lambda=\mu$, it has that the sum of the coefficients in the right hand side of Equations (27a) and (27c) is equal to the coefficient in the right hand side of Equation (27b). That shows the curvature relation for these three curves. These curves are indeed arcs.

For the points of junction, it has

$$
\begin{aligned}
0=&\lambda\left[\frac{\varphi'\varphi_1+\psi'\psi_1}{\sqrt{\varphi'^2+\psi'^2}}\Big|_{t=0}^{t=t^*(0)}+\frac{p'p_1+q'q_1}{\sqrt{p'^2+q'^2}}\Big|_{t=t_c(0)}^{t=T}\right.\\
&\left.+\sqrt{\varphi'^2+\psi'^2}|_{t=t^*(0)}\cdot\frac{\mathrm{d}t^*(\varepsilon)}{\mathrm{d}\varepsilon}|_{\varepsilon=0}-\sqrt{p'^2+q'^2}|_{t=t_c(0)}\cdot\frac{\mathrm{d}t_c(\varepsilon)}{\mathrm{d}\varepsilon}|_{\varepsilon=0}\right]\\
&+\mu\left[\frac{f'f_1+g'g_1}{\sqrt{f'^2+g'^2}}\Big|_{t=t^*(0)}^{t=t_c(0)}\right.\\
&\left.+\sqrt{f'^2+g'^2}|_{t=t_c(0)}\cdot\frac{\mathrm{d}t_c(\varepsilon)}{\mathrm{d}\varepsilon}|_{\varepsilon=0}-\sqrt{f'^2+g'^2}|_{t=t^*(0)}\cdot\frac{\mathrm{d}t^*(\varepsilon)}{\mathrm{d}\varepsilon}|_{\varepsilon=0}\right]\\
&+C(A_{01})\cdot\frac{1}{2}\left[(\varphi\psi_1-\varphi_1\psi)|_{t=0}^{t=t^*(0)}+(fg_1-f_1g)|_{t^*(0)}^{t_c(0)}\right.\\
&+(\varphi\psi'-\varphi'\psi)|_{t=t^*(0)}\cdot\frac{\mathrm{d}t^*(\varepsilon)}{\mathrm{d}\varepsilon}|_{\varepsilon=0}+(fg'-f'g)|_{t_c(0)}\cdot\frac{\mathrm{d}t_c(\varepsilon)}{\mathrm{d}\varepsilon}|_{\varepsilon=0}\\
&\left.-(fg'-f'g)|_{t=t^*(0)}\cdot\frac{\mathrm{d}t^*(\varepsilon)}{\mathrm{d}\varepsilon}|_{\varepsilon=0}\right]\\
&+C(A_{02})\cdot\frac{1}{2}\left[(f_1g-fg_1)|_{t^*(0)}^{t_c(0)}+(p_1q-pq_1)|_{t_c(0)}^{T}\right.\\
&+(f'g-fg'))|_{t=t_c(0)}\cdot\frac{\mathrm{d}t_c(\varepsilon)}{\mathrm{d}\varepsilon}|_{\varepsilon=0}-(f'g-fg')|_{t=t^*(0)}\cdot\frac{\mathrm{d}t^*(\varepsilon)}{\mathrm{d}\varepsilon}|_{\varepsilon=0}\\
&\left.-(p'q-pq')|_{t=t_c(0)}\cdot\frac{\mathrm{d}t_c(\varepsilon)}{\mathrm{d}\varepsilon}|_{\varepsilon=0}\right]. \qquad (28)
\end{aligned}
$$

Specify the data for every point as follows:

$$
\begin{aligned}
0 &= \{\varphi_1, \psi_1\} \cdot \left[\frac{-\lambda\{\varphi', \psi'\}}{\sqrt{\varphi'^2 + \psi'^2}} + \frac{C(A_{01})}{2}\{\psi, -\varphi\} \right] |_{t=0} \\
&+ \left\{ \{\varphi_1, \psi_1\} \cdot \left[\frac{\lambda\{\varphi', \psi'\}}{\sqrt{\varphi'^2 + \psi'^2}} + \frac{C(A_{01})}{2}\{-\psi, \varphi\} \right] \right. \\
&+ \{f_1, g_1\} \cdot \left[-\frac{\mu\{f', g'\}}{\sqrt{f'^2 + g'^2}} + \frac{C(A_{01}) - C(A_{02})}{2}\{g, -f\} \right] \\
&+ \frac{\mathrm{d}t^*(\varepsilon)}{\mathrm{d}\varepsilon}|_{\varepsilon=0} \cdot \left[\lambda\sqrt{\varphi'^2 + \psi'^2} - \mu\sqrt{f'^2 + g'^2} \right. \\
&\left. \left. + \frac{C(A_{01})}{2}((\varphi\psi' - \varphi'\psi) - (fg' - f'g)) + \frac{C(A_{02})}{2}(fg' - f'g) \right] \right\} |_{t=t^*(0)} \\
&+ \left\{ \{p_1, q_1\} \cdot \left[-\frac{\lambda\{p', q'\}}{\sqrt{p'^2 + q'^2}} + \frac{C(A_{02})}{2}\{-q, p\} \right] \right. \\
&+ \{f_1, g_1\} \cdot \left[+\frac{\mu\{f', g'\}}{\sqrt{f'^2 + g'^2}} + \frac{-C(A_{01}) + C(A_{02})}{2}\{g, -f\} \right] \\
&+ \frac{\mathrm{d}t_c(\varepsilon)}{\mathrm{d}\varepsilon}|_{\varepsilon=0} \cdot \left[-\lambda\sqrt{p'^2 + q'^2} + \mu\sqrt{f'^2 + g'^2} \right. \\
&\left. \left. + \frac{C(A_{01})}{2}(fg' - f'g) + \frac{C(A_{02})}{2}((f'g - fg') - (p'q - pq')) \right] \right\} |_{t=t_c(0)} \\
&+ \{p_1, q_1\} \cdot \left[\frac{\lambda\{p', q'\}}{\sqrt{p'^2 + q'^2}} + \frac{C(A_{02})}{2}\{q, -p\} \right] |_{t=T}. \qquad (29)
\end{aligned}
$$

According to the boundary conditions Equations (10) and (12), one can find at $t = t^*(\varepsilon)$ that

$$
\begin{aligned}
&\varphi(t^*(\varepsilon)) + \varepsilon\varphi_1(t^*(\varepsilon)), \psi(t^*(\varepsilon)) + \varepsilon\psi_1(t^*(\varepsilon))\} \\
&\quad = \{f(t^*(\varepsilon)) + \varepsilon f_1(t^*(\varepsilon)), g(t^*(\varepsilon)) + \varepsilon g_1(t^*(\varepsilon))\} \\
&\quad = \{p(T) + \varepsilon p_1(T), q(T) + \varepsilon q_1(T)\}.
\end{aligned}
$$

Compute derivative with respect to ε, then we have at $t = t^*(\varepsilon)(t = T)$ that

$$
\begin{aligned}
&\{\varphi'(t)t^{*'}(\varepsilon) + \varphi_1(t) + \varepsilon\varphi_1'(t)t^{*'}(\varepsilon), \psi'(t) + \psi_1(t) + \varepsilon\psi'_1(t)t^{*'}(\varepsilon)\} \\
&\quad = \{f'(t)t^{*'}(\varepsilon) + f_1(t) + \varepsilon f_1'(t)t^{*'}(\varepsilon), g'(t) + g_1(t) + \varepsilon g'_1(t)t^{*'}(\varepsilon)\} \qquad (30) \\
&\quad = \{p_1(T), q_1(T)\}.
\end{aligned}
$$

By a similar discussion to Equation (30) at $t = t^*(0)(t = T)$, one has analogies for the points $t = t_c(0)(t = t_*(0) = 0)$ from the conditions Equations (10) and (12). There are six tangent vectors in Equation (29), we rewrite them individually:

$$
\begin{aligned}
&\{\varphi_1, \psi_1\} \cdot \frac{-\lambda\{\varphi', \psi'\}}{\sqrt{\varphi'^2 + \psi'^2}}|_{t=0} \\
&+ \left[\{\varphi_1, \psi_1\} \cdot \frac{\lambda\{\varphi', \psi'\}}{\sqrt{\varphi'^2 + \psi'^2}} + \{f_1, g_1\} \cdot \frac{-\mu\{f', g'\}}{\sqrt{f'^2 + g'^2}} \right] |_{t=t^*(0)}
\end{aligned}
$$

$$
\begin{aligned}
&+\left[\{p_1,q_1\}\cdot\frac{-\lambda\{p',q'\}}{\sqrt{p'^2+q'^2}}+\{f_1,g_1\}\cdot\frac{\mu\{f',g'\}}{\sqrt{f'^2+g'^2}}\right]|_{t=t_c(0)}\\
&+\{p_1,q_1\}\cdot\frac{\lambda\{p',q'\}}{\sqrt{p'^2+q'^2}}|_{t=T}\\
&=\{\varphi_1,\psi_1\}\cdot\frac{-\lambda\{\varphi',\psi'\}}{\sqrt{\varphi'^2+\psi'^2}}|_{t=0}\\
&+\left[\{p_1(T)-\varphi'(t^*(0))t^{*'}(\varepsilon),q_1(T)-\psi'(t^*(0))t^{*'}(\varepsilon)\}\cdot\frac{\lambda\{\varphi'(t^*(0)),\psi'(t^*(0))\}}{\sqrt{\varphi'^2(t^*(0))+\psi'^2(t^*(0))}}\right.\\
&\left.+\{p_1(T)-f'(t^*(0))t^{*'}(\varepsilon),q_1(T)-g'(t^*(0))t^{*'}(\varepsilon)\}\cdot\frac{-\mu\{f'(t^*(0)),g'(t^*(0))\}}{\sqrt{f'^2(t^*(0))+g'^2(t^*(0))}}\right]|_{\varepsilon=0}\\
&+v\left[\{\varphi_1(0)-p'(t_c(0))t_c'(\varepsilon),\psi_1(0)-q'(t_c(0))t_c'(\varepsilon)\}\cdot\frac{-\lambda\{p'(t_c(0)),q'(t_c(0))\}}{\sqrt{p'^2(t_c(0))+q'^2(t_c(0))}}\right.\\
&\left.+\{\varphi_1(0)-f'(t_c(0))t_c'(\varepsilon),\psi_1(0)-g'(t_c(0))t_c'(\varepsilon)\}\cdot\frac{\mu\{f'(t_c(0)),g'(t_c(0))\}}{\sqrt{f'^2(t_c(0))+g'^2(t_c(0))}}\right]|_{\varepsilon=0}\\
&+\{p_1(T),q_1(T)\}\cdot\frac{\lambda\{p'(T),q'(T)\}}{\sqrt{p'^2(T)+q'^2(T)}}\\
&=\{\varphi_1(0),\psi_1(0)\}\cdot\frac{-\lambda\{\varphi'(0),\psi'(0)\}}{\sqrt{\varphi'^2(0)+\psi'^2(0)}}\\
&+\{p_1(T),q_1(T)\}\cdot\left[\frac{\lambda\{\varphi'(t^*(0)),\psi'(t^*(0))\}}{\sqrt{\varphi'^2(t^*(0))+\psi'^2(t^*(0))}}-\frac{\mu\{f'(t^*(0)),g'(t^*(0))\}}{\sqrt{f'^2(t^*(0))+g'^2(t^*(0))}}\right]\\
&+\left[-\lambda\sqrt{\varphi'^2(t^*(0))+\psi'^2(t^*(0))}+\mu\sqrt{f'^2(t^*(0))+g'^2(t^*(0))}\right]\cdot t^{*'}(\varepsilon)|_{\varepsilon=0}\\
&+\{\varphi_1(0),\psi_1(0)\}\cdot\left[\frac{-\lambda\{p'(t_c(0)),q'(t_c(0))\}}{\sqrt{p'^2(t_c(0))+q'^2(t_c(0))}}+\frac{\mu\{f'(t_c(0)),g'(t_c(0))\}}{\sqrt{f'^2(t_c(0))+g'^2(t_c(0))}}\right]\\
&+\left[\lambda\sqrt{p'^2(t_c(0))+q'^2(t_c(0))}-\mu\sqrt{f'^2(t_c(0))+g'^2(t_c(0))}\right]\cdot t_c'(\varepsilon)|_{\varepsilon=0}\\
&+\{p_1(T),q_1(T)\}\cdot\frac{\lambda\{p'(T),q'(T)\}}{\sqrt{p'^2(T)+q'^2(T)}}
\end{aligned}
\tag{31}
$$

Let us see the terms with the coefficients $C(A_{01})$ and $C(A_{02})$ at the junctions in Equation (29), it has

$$
\begin{aligned}
&\{\varphi_1,\psi_1\}\cdot\left[\frac{C(A_{01})}{2}\{\psi,-\varphi\}\right]|_{t=0}\\
&+\left\{\{\varphi_1,\psi_1\}\cdot\left[\frac{C(A_{01})}{2}\{-\psi,\varphi\}\right]+\{f_1,g_1\}\cdot\left[\frac{C(A_{01})-C(A_{02})}{2}\{g,-f\}\right]\right.\\
&\left.+\frac{\mathrm{d}t^*(\varepsilon)}{\mathrm{d}\varepsilon}|_{\varepsilon=0}\cdot\left[\frac{C(A_{01})}{2}((\varphi\psi'-\varphi'\psi)-(fg'-f'g))+\frac{C(A_{02})}{2}(fg'-f'g)\right]\right\}|_{t=t^*(0)}
\end{aligned}
$$

$$
\begin{aligned}
&+\left\{\{p_1,q_1\}\cdot\left[\frac{C(A_{02})}{2}\{-q,p\}\right]+\{f_1,g_1\}\cdot\left[\frac{-C(A_{01})+C(A_{02})}{2}\{g,-f\}\right]\right.\\
&\left.+\frac{\mathrm{d}t_c(\varepsilon)}{\mathrm{d}\varepsilon}|_{\varepsilon=0}\cdot\left[\frac{C(A_{01})}{2}(fg'-f'g)+\frac{C(A_{02})}{2}((f'g-fg')-(p'q-pq'))\right]\right\}|_{t=t_c(0)}\\
&+\{p_1,q_1\}\cdot\left[\frac{C(A_{02})}{2}\{q,-p\}\right]|_{t=T}\\
&=\{\varphi_1,\psi_1\}\cdot\left[\frac{C(A_{01})}{2}\{\psi,-\varphi\}\right]|_{t=0}\\
&+\left\{\{\varphi_1,\psi_1\}\cdot\left[\frac{C(A_{01})}{2}\{-\psi,\varphi\}\right]+\{f_1,g_1\}\cdot\left[\frac{C(A_{01})-C(A_{02})}{2}\{g,-f\}\right]\right.\\
&+\left[\frac{C(A_{01})}{2}(\varphi(q_1(T)-\psi_1)-(p_1(T)-\varphi_1)\psi)\right.\\
&\left.\left.+\frac{C(A_{02})-C(A_{01})}{2}(f(q_1(T)-g_1)-(p_1(T)-f_1)g)\right]\right\}|_{t=t^*(0)}\\
&+\left\{\{p_1,q_1\}\cdot\left[\frac{C(A_{02})}{2}\{-q,p\}\right]+\{f_1,g_1\}\cdot\left[\frac{-C(A_{01})+C(A_{02})}{2}\{g,-f\}\right]\right.\\
&+\left[\frac{C(A_{01})-C(A_{02})}{2}(f(\psi_1(0)-g_1)-(\varphi_1(0)-f_1)g)\right.\\
&\left.\left.-\frac{C(A_{02})}{2}((\varphi_1(0)-p_1)q-p(\psi_1(0)-q_1))\right]\right\}|_{t=t_c(0)}\\
&+\{p_1,q_1\}\cdot\left[\frac{C(A_{02})}{2}\{q,-p\}\right]|_{t=T}\\
&=\{\varphi_1,\psi_1\}\cdot\left[\frac{C(A_{01})}{2}\{\psi,-\varphi\}\right]|_{t=0}\\
&+\left\{\{f_1,g_1\}\cdot\left[\frac{C(A_{01})-C(A_{02})}{2}\{g,-f\}\right]\right.\\
&\left.+\left[\frac{C(A_{01})}{2}(\varphi\cdot q_1(T)-p_1(T)\cdot\psi)+\frac{C(A_{02})-C(A_{01})}{2}(f(q_1(T)-g_1)-(p_1(T)-f_1)g)\right]\right\}|_{t=t^*(0)}\\
&+\left\{\{f_1,g_1\}\cdot\left[\frac{-C(A_{01})+C(A_{02})}{2}\{g,-f\}\right]\right.\\
&\left.+\left[\frac{C(A_{01})-C(A_{02})}{2}(f(\psi_1(0)-g_1)-(\varphi_1(0)-f_1)g)-\frac{C(A_{02})}{2}(\varphi_1(0)\cdot q-p\cdot\psi_1(0))\right]\right\}|_{t=t_c(0)}\\
&+\{p_1,q_1\}\cdot\left[\frac{C(A_{02})}{2}\{q,-p\}\right]|_{t=T}\\
&=\{\varphi_1,\psi_1\}\cdot\left[\frac{C(A_{01})}{2}\{\psi,-\varphi\}\right]|_{t=0}\\
&+\left\{\{f_1,g_1\}\cdot\left[\frac{C(A_{01})-C(A_{02})}{2}\{g,-f\}\right]\right.
\end{aligned}
$$

$$
\begin{aligned}
&+\left[\frac{C(A_{02})}{2}(f(q_1(T)-g_1)-(p_1(T)-f_1)g)+\frac{C(A_{01})}{2}(fg_1-f_1g)\right]\Bigg\}|_{t=t^*(0)}\\
&+\left\{\{f_1,g_1\}\cdot\left[\frac{-C(A_{01})+C(A_{02})}{2}\{g,-f\}\right]\right.\\
&\left.+\left[\frac{C(A_{01})-C(A_{02})}{2}(f(\psi_1(0)-g_1)-(\varphi_1(0)-f_1)g)-\frac{C(A_{02})}{2}(\varphi_1(0)\cdot q-p\cdot\psi_1(0))\right]\right\}|_{t=t_c(0)}\\
&+\{p_1,q_1\}\cdot\left[\frac{C(A_{02})}{2}\{q,-p\}\right]|_{t=T}\\
&=\{\varphi_1,\psi_1\}\cdot\left[\frac{C(A_{01})}{2}\{\psi,-\varphi\}\right]|_{t=0}\\
&+\left\{\{f_1,g_1\}\cdot\left[\frac{-C(A_{02})}{2}\{g,-f\}\right]+\left[\frac{C(A_{02})}{2}(f(q_1(T)-g_1)-(p_1(T)-f_1)g)\right]\right\}|_{t=t^*(0)}\\
&+\left\{\left[\frac{C(A_{01})-C(A_{02})}{2}(f\cdot\psi_1(0)-\varphi_1(0)\cdot g)-\frac{C(A_{02})}{2}(\varphi_1(0)\cdot q-p\cdot\psi_1(0))\right]\right\}|_{t=t_c(0)}\\
&+\{p_1,q_1\}\cdot\left[\frac{C(A_{02})}{2}\{q,-p\}\right]|_{t=T}\\
&=\{\varphi_1,\psi_1\}\cdot\left[\frac{C(A_{01})}{2}\{\psi,-\varphi\}\right]|_{t=0}+\frac{C(A_{01})}{2}\{\varphi_1(0),\psi_1(0)\}\cdot\{-g,f\}|_{t=t_c(0)}\\
&=0.
\end{aligned}
\tag{32}
$$

Equation (32) tells us that it becomes zero combining all terms including $C(A_{01})$ and $C(A_{02})$ in Equation (29). And, by using Equations (32), (29), and (29), it follows that Equation (27) satisfies

$$
\begin{aligned}
&\{\varphi_1(0),\psi_1(0)\}\cdot\\
&\left[\frac{-\lambda\{\varphi'(0),\psi'(0)\}}{\sqrt{\varphi'^2(0)+\psi'^2(0)}}+\frac{\mu\{f'(t_c(0)),g'(t_c(0))\}}{\sqrt{f'^2(t_c(0))+g'^2(t_c(0))}}+\frac{-\lambda\{p'(t_c(0)),q'(t_c(0))\}}{\sqrt{p'^2(t_c(0))+q'^2(t_c(0))}}\right]\\
&+\{p_1(T),q_1(T)\}\cdot\\
&\left[\frac{\lambda\{\varphi'(t^*(0)),\psi'(t^*(0))\}}{\sqrt{\varphi'^2(t^*(0))+\psi'^2(t^*(0))}}-\frac{\mu\{f'(t^*(0)),g'(t^*(0))\}}{\sqrt{f'^2(t^*(0))+g'^2(t^*(0))}}+\frac{\lambda\{p'(T),q'(T)\}}{\sqrt{p'^2(T)+q'^2(T)}}\right]\\
&=0.
\end{aligned}
\tag{33}
$$

Using the notations

$$
\mathbf{T}_{01}=\frac{\{\varphi'(0),\psi'(0)\}}{\sqrt{\varphi'^2(0)+\psi'^2(0)}},\qquad \mathbf{T}_{11}=\frac{\{\varphi'(t^*(0)),\psi'(t^*(0))\}}{\sqrt{\varphi'^2(t^*(0))+\psi'^2(t^*(0))}},\tag{34a}
$$

$$
\mathbf{T}_{02}=\frac{\{f'(t_c(0)),g'(t_c(0))\}}{\sqrt{f'^2(t_c(0))+g'^2(t_c(0))}},\qquad \mathbf{T}_{12}=\frac{\{f'(t^*(0)),g'(t^*(0))\}}{\sqrt{f'^2(t^*(0))+g'^2(t^*(0))}},\tag{34b}
$$

$$
\mathbf{T}_{03}=\frac{\{p'(t_c(0)),q'(t_c(0))\}}{\sqrt{p'^2(t_c(0))+q'^2(t_c(0))}},\qquad \mathbf{T}_{13}=\frac{\{p'(T),q'(T)\}}{\sqrt{p'^2(T)+q'^2(T)}}\tag{34c}
$$

and the arbitrariness of vectors $\{\varphi_1(0),\psi_1(0)\}$ and $\{p_1(T),q_1(T)\}$, Equation (33) becomes

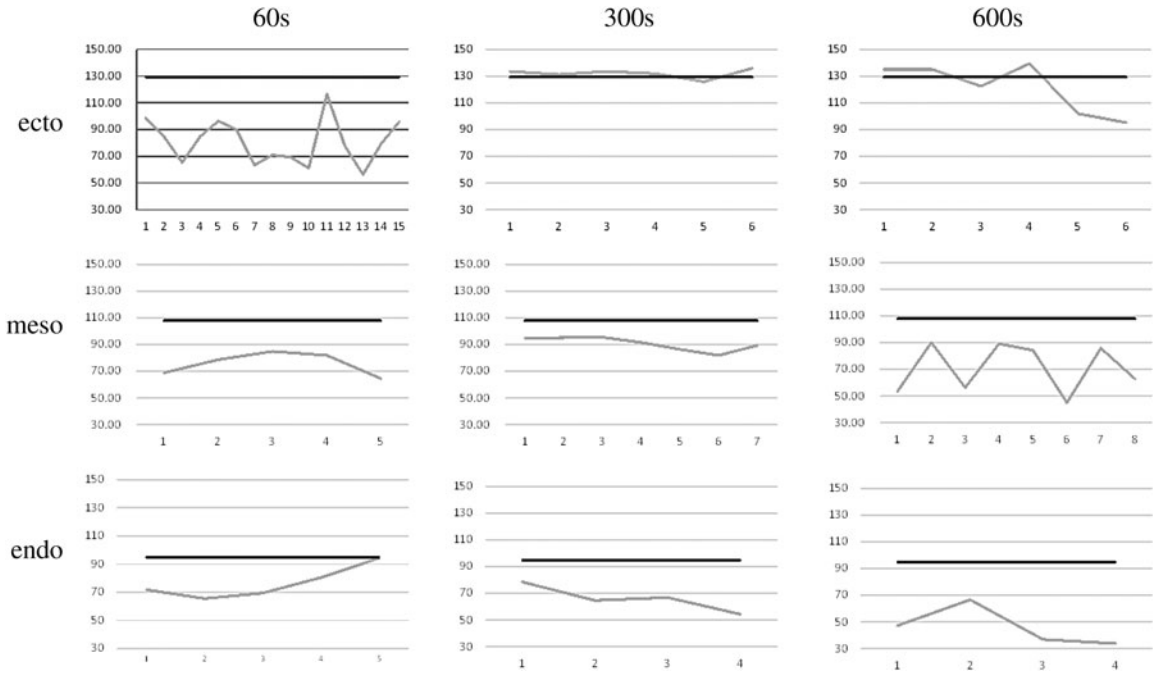

FIG. 7. Experimental values of θ are usually lower than the theoretic values (horizontal lines) for three record times: 60, 300, and 600 s. The contact angle θ results from the balance between the adhesion tension and the cortex tensions for homotypic ectoderm (ecto), mesoderm (meso), and endoderm (endo) doublets during contact formation.

$$-\lambda\mathbf{T}_{01}+\mu\mathbf{T}_{02}-\lambda\mathbf{T}_{03}=0, \tag{35a}$$

$$\lambda\mathbf{T}_{11}-\mu\mathbf{T}_{12}+\lambda\mathbf{T}_{13}=0. \tag{35b}$$

By solving Equation (35), one gets

$$\cos\theta_{12}=\cos\theta_{23}=\langle\mathbf{T}_{01},\mathbf{T}_{02}\rangle=\langle\mathbf{T}_{11},\mathbf{T}_{12}\rangle=\langle\mathbf{T}_{02},\mathbf{T}_{03}\rangle=\langle\mathbf{T}_{12},\mathbf{T}_{13}\rangle=\frac{\mu}{2\lambda}, \tag{36a}$$

$$\cos\theta_{13}=\langle\mathbf{T}_{01},\mathbf{T}_{03}\rangle=\langle\mathbf{T}_{11},\mathbf{T}_{13}\rangle=-1+\frac{\mu^2}{2\lambda^2}. \tag{36b}$$

TABLE 2. DISTRIBUTION FOR THE DATA OF THE *DROSOPHILA* EYE

No.	*Group*	*Frequency*	*Probability*	*Gauss*	*Error*
1	(0, 120]	0	0.000000	0.001607	–0.001607
2	(120, 123.89]	1	0.004717	0.005432	–0.000715
3	(123.89, 127.78]	2	0.009434	0.015276	–0.005842
4	(127.78, 131.67]	6	0.028302	0.035748	–0.007446
5	(131.67, 135.56]	13	0.061321	0.069618	–0.008297
6	(135.56, 139.45]	19	0.089623	0.112821	–0.023198
7	(139.45, 143.34]	28	0.132075	0.152148	–0.020073
8	(143.34, 147.23]	31	0.146226	0.170746	–0.024520
9	(147.23, 151.12]	36	0.169811	0.159456	0.010355
10	(151.12, 155.01]	31	0.146226	0.123919	0.022307
11	(155.01, 158.9]	22	0.103774	0.080139	0.023635
12	(158.9, 162.79]	12	0.056604	0.043127	0.013477
13	(162.79, 166.68]	8	0.037736	0.019314	0.018422
14	(166.68, 170.57]	2	0.009434	0.007198	0.002236
15	(170.57, 176]	0	0.000000	0.001335	–0.001335

"Gauss" represents the value of corresponding Gaussian distribution.

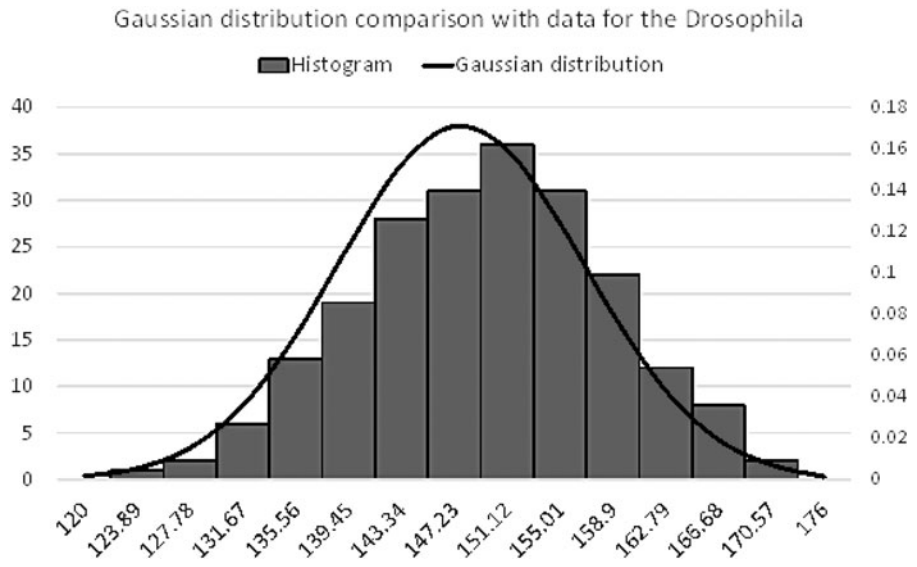

FIG. 8. Angle distribution of *Drosophila* cells.

6. APPENDIX A2: SOME DATA EXAMPLES

Zebrafish gastrulation cell, epithelia cell in *Drosophila* retina, and cells of two green algae including *Pediastrum* and *Tretrastrum* are used to test our model.

6.1. Cell sorting in zebrafish gastrulation

Maîstre et al. (2012) described the size of the cell–cell contact determined by the balance of forces (cell adhesion and cortex tension) at the contact boundary: $\cos(\theta) = \gamma_i/(2\gamma_{cm})$ (where $\gamma_i = 2\gamma_{cc} - \omega$). Here, the contact angle θ results from the balance between the adhesion tension ω and the cortex tensions at the cell–medium γ_{cm} and cell–cell interfaces γ_{cc} during zebrafish gastrulation. We find there are some angle errors between the theoretic values by $\arccos\frac{\gamma_i}{2\gamma_{cm}}$ and the corresponding measurement values, the latter is usually lower than the former (Fig. 7).

Table 3. Compare Gaussian with the Distribution for Outer Angle θ

No.	*Degree*	*Group*	*Frequency*	*Probability*	*Gauss*	*Error*
1	35	(0, 35]	0	0	0.001534488	–0.00153
2	45	(35, 45]	1	0.014925	0.004975289	0.00995
3	55	(45, 55]	1	0.014925	0.013607338	0.001318
4	65	(55, 65]	1	0.014925	0.031392641	–0.01647
5	75	(65, 75]	1	0.014925	0.061091721	–0.04617
6	85	(75, 85]	5	0.074627	0.100285172	–0.02566
7	95	(85, 95]	7	0.104478	0.138864402	–0.03439
8	105	(95, 105]	14	0.208955	0.162197807	0.046757
9	115	(105, 115]	5	0.074627	0.159808132	–0.08518
10	125	(115, 125]	17	0.253731	0.132816679	0.120915
11	135	(125, 135]	5	0.074627	0.093112117	–0.01849
12	145	(135, 145]	7	0.104478	0.05506297	0.049415
13	155	(145, 155]	3	0.044776	0.027467107	0.017309
14	165	(155, 165]	0	0	0.011557557	–0.01156

The angle θ is the outer angle at every junction on the outer boundaries of cells of *Pediastrum.*

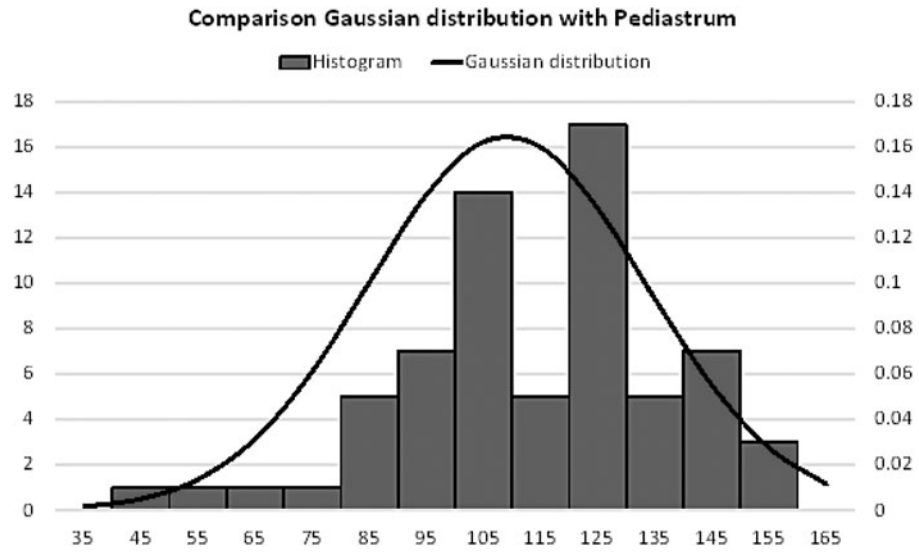

FIG. 9. The outer angles distribution for Pediastrum cells.

6.2. *Cell geometric order in the* Drosophila *eye*

Now we consider the *Drosophila* eye as an example. Chan et al. (2017) tried to establish a quantitative link between adhesion and contractility and reveal the role of N-cadherin on cell shapes and cell arrangements. And they designed a 2D model based on the minimization of a tension-based energy function (Käfer et al., 2007; Hilgenfeldt et al., 2008). We show the analysis results for the data of Chan et al. (2017) in Table 2 and find a deviation between the suggested value of $\theta_3 = 130^\circ$ and the average value of experimental data.

The average value for the contact angles $\theta = \theta_3$ is 147.73°. The group of these angles covers from an interval [121.16°, 171.18°], and follows Gaussian distribution (Fig. 8). An interesting fact shows that the

Table 4. All Data for 25 Pictures (104 Angles) for *Tetrastrum* Cells

[I] Tetr1	*[I] Tetr2*	*[I] Tetr3*	*[I] Tetr4*	*[I] Tetr5*	*[I] Tetr6*	*[I] Tetr7*
101.31	113.02	123.11	124.08	99.22	117.76	127.94
116.83	100.96	120.26	109.94	70.03	92.12	128.29
117.38	97.00	111.80	128.88	112.22	83.28	97.27
122.28	133.67	122.66	128.79	76.14	89.82	77.04
[K] Fig. b	*[K] Fig. c*	*[K] Fig. d*	*[A] Fig. 1*	*[A] Fig. 2*	*[A] Fig. 3*	*[A] Fig. 4*
119.29	111.93	102.09	110.3764	99.16235	116.5651	85.42608
84.95	116.57	97.48	64.44003	90	98.97263	90
116.57	135.00	137.29	83.65981	90	88.66778	75.96376
100.01	104.54	109.46	144.4623	82.87498	68.19859	88.15239
[A] Fig. 5	*[A] Fig. 6*	*[A] Fig. 7*	*[A] Fig. 8*	*[A] Fig. 10*	*[A] Fig. 12*	*[A] Fig. 14*
81.02737	96.54629	94.57392	90	64.44003	70.34618	59.0362
75.96376	90	107.1027	56.30993	105.2551	120.9638	101.3099
75.96376	101.3099	79.50852	71.56505	81.02737	78.69007	98.1301
129.0939	85.60129	82.23483	72.89727	75.96376	90	101.8887
[A] Fig. 15	*[A] Fig. 16*	*[A] Fig. 19*	*[A] Fig. 20*			
90	120.3236	69.30455	93.36646			
99.46232	91.78991	79.50852	98.1301			
98.1301	90	99.18884	98.1301			
106.5873	110.2249	75.96376	94.39871			

TABLE 5. DISTRIBUTION OF THE ANGLES OF *TETRASTRUM* CELLS

No.	*Degree*	*Group*	*Frequency*	*Probability*	*Gauss*	*Error*
1	55	(0, 55]	0	0	0.001567356	–0.00157
2	62.5	(55, 62.5]	2.00	0.019230769	0.003528326	0.015702
3	70	(62.5, 70]	4.00	0.038461538	0.006819568	0.031642
4	77.5	(70, 77.5]	11.00	0.105769231	0.011317024	0.094452
5	85	(77.5, 85]	10.00	0.096153846	0.016124818	0.080029
6	92.5	(85, 92.5]	15.00	0.144230769	0.019726254	0.124505
7	100	(92.5, 100]	16.00	0.153846154	0.020719612	0.133127
8	107.5	(100, 107.5]	12.00	0.115384615	0.018685546	0.096699
9	115	(107.5, 115]	10.00	0.096153846	0.01446829	0.081686
10	122.5	(115, 122.5]	11.00	0.105769231	0.009618687	0.096151
11	130	(122.5, 130]	9.00	0.086538462	0.005490369	0.081048
12	137.5	(130, 137.5]	3.00	0.028846154	0.002690757	0.026155
13	145	(137.5, 145]	1.00	0.009615385	0.00113223	0.008483
14	152.5	(145, 152.5]	0.00	0	0.000409055	–0.00041

confidence interval under a confidence level of 95% is $(146.51° - 148.95°)$. This interval has a difference with its theoretic value $(121° - 139°)$ $(\theta_3 = 130° \pm 9°)$ of Chan et al. (2017).

6.3. *Comparison of Gaussian distribution with* Pediastrum

Here, eight pictures (see ''Section 1. Measuremental data for *Pediastrum* cells'' in Supplementary Materials for *Pediastrum* cell images) of *Pediastrum* cells taken by our research group are used to investigate the distribution for the outer angles.

The angles are labeled clockwise beginning with the top angle (see image0140 in Section 1 ''Measuremental data for Pediastrum cells'' of Supplementary Materials). The data include 67 angles with minimum 37.07° and maximum 152.93°, and the average (mathematical expectation) is 109.13°. One can find the distribution in Table 3 and Figure 9.

The confidence interval under a confidence level of 95% is $105.467° - 112.80°$. The average value $109.13° < 2\pi/3$.

6.4. *Analysis on distribution for* Tetrastrum *cells*

We borrow the data from literature (Ahlstrom and Tiffany 1934; Krienitz and Wachsmuth, 1991) and Internet resources (Supplementary Materials) for analysis.

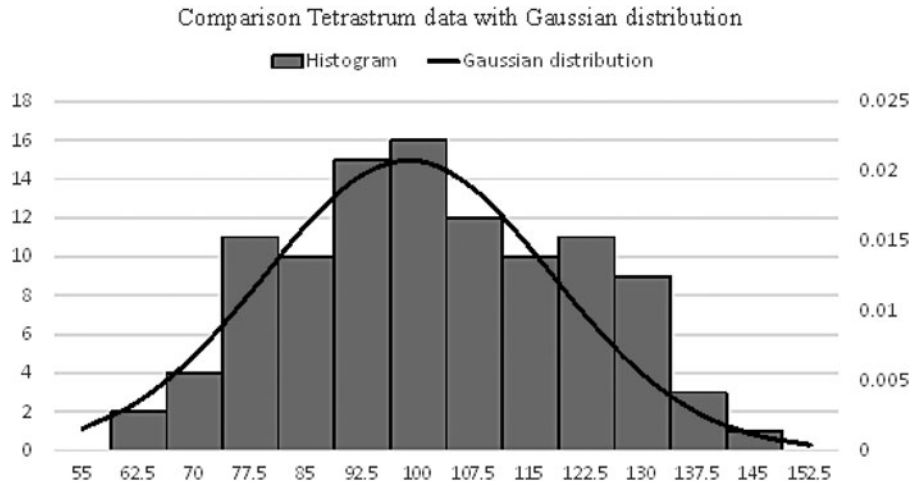

FIG. 10. The distribution for the angles of *Tetrastrum* cells.

The angles are labeled clockwise beginning with the top angle, as for the *Pediastrum* (see ''Section 2. How to label the angle for *Tetrastrum* and Internet resources'' in Supplementary Materials). The data include 104 angles with minimum 56.31° and maximum 144.46°, and the average is 98.67°. One can find the distribution in Tables 4 and 5 and Figure 10. The notations [A], [K], and [I] in Table 4 indicate the references (Ahlstrom and Tiffany, 1934; Krienitz and Wachsmuth, 1991) and Internet resources (Supplementary Materials), respectively.

ACKNOWLEDGMENT

The authors thank Prof. Jian Li in Shanghai University for his help in preparation of experiments.

AUTHOR DISCLOSURE STATEMENT

The authors declare that no conflicting financial interests exist.

REFERENCES

Ahlstrom, E.H., and Tiffany, L.H. 1934. The algal genus tetrastrum. *Am. J. Bot.* 21, 499–507.

Besson, S., and Dumais, J. 2011. Universal rule for the symmetric division of plant cells. *Proc. Natl. Acad. Sci. U. S. A.* 108, 6294–6299.

Chan, H.Y., Shivakumar, P.C., Clément, R., et al. 2017. Patterned cortical tension mediated by N-cadherin controls cell geometric order in the *Drosophila* eye. *eLife*. 6; DOI: 10.7554/eLife.22796.

Cox, C., Harrison, L., Hutchings, M., et al. 1994. The shortest enclosure of three connected areas in R^2. *Real Anal. Exch.* 20, 313–335.

Dupuy, L., Mackenzie, J., and Haseloff, J. 2010. Coordination of plant cell division and expansion in a simple morphogenetic system. *Proc. Natl. Acad. Sci. U. S. A.* 107, 2711–2716.

Foisy, J., Alfaro, M., Brock, J., et al. 1993. The standard double soap bubble in R^2 uniquely minimizes perimeter. *Pac. J. Math.* 159, 47–59.

Fukushima, K., Fujita, H., Yamaguchi, T., et al. 2015. Oriented cell division shapes carnivorous pitcher leaves of Sarracenia purpurea. *Nat. Commun.* 6, 6450.

Gawlik, S.R., and Millington, W.F. 1969. Pattern formation and the fine structure of the developing cell wall in colonies of *Pediastrum boryanum*. *Am. J. Bot.* 56, 1084–1093.

Gemp, I.M., Carthew, R.W., and Hilgenfeldt, S. 2011. Cadherin-dependent cell morphology in an epithelium: Constructing a quantitative dynamical model. *PLoS Comput. Biol.* 7, e1002115.

Goldberg, M. 1969. Elementary problems: E2185. *Am. Math. Mon.* 76, 825.

Haig D. 2015. Coleochaete and the origin of sporophytes. *Am. J. Bot.* 102, 417–422.

Hayashi, T., and Carthew, R.W. 2004. Surface mechanics mediate pattern formation in the developing retina. *Nature* 431, 647–652.

Hilgenfeldt, S., Erisken, S., and Carthew R.W. 2008. Physical modeling of cell geometric order in an epithelial tissue. *Proc. Natl. Acad. Sci. U. S. A.* 105, 907–911.

Käfer, J.K., Hayashi, T., Mareé, A.F.M., et al. 2007. Cell adhesion and cortex contractility determine cell patterning in the *Drosophila* retina. *Proc. Natl. Acad. Sci. U. S. A.* 104, 18549–18554.

Karol, K.G., McCourt, R.M., Cimino, M.T., et al. 2001. The Closest living relatives of land plants. *Science* 294:2351–2353.

Klamkin, M.S. 1992. Book reviews. *SIAM Rev.* 34, 335–338.

Krienitz, L., and Wachsmuth, G. 1991. Zur variabilität der zellwandornamentierung in der gattung *Tetrastrum* Chodat (Chlorophyceae, Chlorellales) und einige taxonomische schlußfolgerungen. *Arch. Protistenkunde.* 139, 39–51.

Maître, J.-L., Berthoumieux, H., Krens, S., et al. 2012. Adhesion functions in cell sorting by mechanically coupling the cortices of adhering cells. *Science* 338, 253–256.

Millington, W.F., Chubb, G.T., and Seed, T.M. 1981. Cell shape in the alga *Pediastrum* (*Hydrodictyaceae*; *Chlorophyta*). *Protoplasma* 105, 169–176.

Morgan, F. 2009. *Geometric Measure Theory: A Beginner's Guide*, 4th ed. Academic Press, London.

Rasmussen, C.G., Wright, A.J., and Müller, S. 2013. The role of the cytoskeleton and associated proteins in determination of the plant cell division plane. *Plant J.* 75, 258–269.

Ruhfel, B.R., Gitzendanner, M.A., Soltis, P.S., et al. 2014. From algae to angiosperms-inferring the phylogeny of green plants (Viridiplantae) from 360 plastid genomes. *BMC Evol. Biol.* 14, 23.

Shi, B.L., and Wang, Y.D. 2012. Evolution modeling on growth image of cells. *Comput. Simul.* 29, 307–311 (in Chinese).

Sinnott, E.M., and Bloch, R. 1940. Cytoplasmic behavior during division of vacuolate plant cells. *Proc. Natl. Acad. Sci. U. S. A.* 26, 223–227.

Smith, L.G. 2001. Plant cell division: Building walls in the right places. *Nat. Rev. Mol. Cell Biol.* 2, 33–39.

Timme, R.E., and Delwiche, C.F. 2010. Uncovering the evolutionary origin of plant molecular processes: Comparison of *Coleochaete* (Coleochaetales) and *Spirogyra* (Zygnematales) transcriptomes. *BMC Plant Biol.* 10, 96.

Wang, Y.D., and Cong, J.Y. 2016. An improved model of non-uniform *Coleochaete* cell division. *J. Comput. Biol.* 23, 693–709.

Wang, Y.D., Dou, M.Y., and Zhou, Z.G. 2015. The fencing problem and *Coleochaete* cell division. *J. Math. Biol.* 70, 893–912.

Wang, Y.D., and Zeng, K. 2018. Analysis on mechanism for edge formation for *Coleochaete* cell in non-uniform division. *J. Math. Pract. Theory* (in Chinese), accepted.

Wesley, O.C. 1928. Asexual reproduction in *Coleochaete. Bot. Gaz.* 86, 1–31.

Wichiramala, W. 2004. Proof of the planar triple bubble conjecture. *J. Reine Angew. Math.* 567, 1–49.

Wiener, N. 1914. The shortest line dividing an area in a given ratio. *Proc. Camb. Philos. Soc.* 18, 56–58.

Yang, J.G. 1986. *Coleochaete* and the origin of terrestrial plants. *Chin. Bull. Bot.* 4, 114–116) (in Chinese).

Address correspondence to:
Dr. Yuandi Wang
Department of Mathematics
Shanghai University
Shanghai 200444
China

E-mail: ydwang@shu.edu.cn